Forces in Wingwalls from Thermal Expansion of Skewed Semi-Integral Bridges

Eric Steinberg, Ph.D., P.E.
Shad Sargand, Ph.D.

for the
Ohio Department of Transportation
Office of Research and Development

and the
Federal Highway Administration

State Job Number 134267

November, 2010

Ohio Research Institute for
Transportation and the Environment

1. Report No.	2. Government Accession No.	3. Recipient's Catalog No.
FHWA/OH-2010/16		

4. Title and subtitle	5. Report Date
Forces on Wingwalls from Thermal Expansion of Skewed Semi-Integral Bridges	**November 2010**
	6. Performing Organization Code

7. Author(s)	8. Performing Organization Report No.
Eric Steinberg **Shad Sargand**	
	10. Work Unit No. (TRAIS)

9. Performing Organization Name and Address	11. Contract or Grant No.
Ohio University **Ohio Research Institute for Transportation and the Environment** **Department of Civil Engineering** **Athens, OH 45701**	**134267**
	13. Type of Report and Period Covered

12. Sponsoring Agency Name and Address	14. Sponsoring Agency Code
Ohio Department of Transportation **1980 West Broad Street** **Columbus, Ohio 43223**	

15. Supplementary Notes

16. Abstract: Jointless bridges, such as semi-integral and integral bridges, have become more popular in recent years because of their simplicity in the construction and the elimination of high costs related to joint maintenance. Prior research has shown that skewed semi-integral bridges tend to expand and rotate as the ambient air temperature increases through the season. As a result of the bridge movement, forces are generated and transferred to the wingwalls of the bridge. ODOT does not currently have a procedure to determine the forces generated in the wingwalls from the thermal expansion and rotation of skewed semi-integral bridges. In this study, two semi-integral bridges with skews were instrumented and monitored for behavior at the interface of the bridge's diaphragm and wingwall. A parametric analysis was also performed to determine the effects of different spans and bridge lengths on he magnitude of the forces. Based on the field results from the study it is recommended for the design of the wingwalls turned to run nearly parallel with the longitudinal axis of skewed semi-integral bridges should include a 100 psi loading at the wingwall/diaphragm interface from the thermal expansion of the bridge. In addition, analytical evaluations showed that longer spans and higher skews than allowed by ODOT's BDM could be used. However, additional considerations for larger movements and stresses generated at the wingwall/diaphragm interface would need to be considered in designs. Finally, bearing retainers in diaphragms, if used, require adequate cover to avoid spalling of concrete.

17. Key Words: Semi-intregral Bridge, Skewed Bridge, Wingwall, Thermal Expansion, Bridge rotation, and Bridge Diaphragm.	18. Distribution Statement No restrictions. This document is available to the public through the National Technical Information Service, Springfield, Virginia 22161

19. Security Classif. (of this report)	20. Security Classif. (of this page)	21. No. of Pages	22. Price
Unclassified	Unclassified		

Forces in Wingwalls from Thermal Expansion of Skewed Semi-Integral Bridges

Final Report

Prepared in Cooperation with the
Ohio Department of Transportation,
U.S. Department of Transportation, and
Federal Highway Administration

Principal Investigators:
Eric Steinberg, Ph.D., P.E.
Shad Sargand, Ph.D.

Ohio University
Ohio Research Institute for Transportation and the Environment
Department of Civil Engineering
Athens, Ohio

November, 2010

ACKNOWLEDGEMENTS

The authors especially thank Jawdat Siddiqi, the ODOT technical liaison, for his insight and input related to the research. The efforts of former graduate student, Jibril Shehu, are also greatly appreciated. The assistance in instrumentation from Dr. Masada and research engineer Issam Khoury of Ohio University also deserve recognition.

TABLE OF CONTENTS

LIST OF FIGURES

LIST OF TABLES

CHAPTER 1: INTRODUCTION

1.1 Background

Bridges that utilize expansion joints have increased the overall maintenance cost of bridges due to leakage at the expansion joint. One of the major causes of expansion joint deterioration is observed when water carrying de-icing salts leaks through the expansion joints. The de-icing salts cause an increased rate of corrosion of the joint, as well as structural components beneath the joint including the superstructure and substructure.

However with the introduction of the jointless bridges such as semi-integral and integral bridges, the high joint maintenance cost is eliminated. In addition, the added simplicity in the construction of integral and semi-integral bridges has led them to become more popular in recent years (Bettinger, 2001). Oesterle and Lotfi (2005) also confirmed that in addition to reduced maintenance cost, jointless bridges improve riding quality, promote lower impact loads, reduce snowplow damage to decks and approach slabs, as well as improve the seismic resistance of the bridge.

Integral bridges are those designed such that the superstructure (deck, girder and diaphragm) are rigidly connected to the substructure through bonded construction joints between the diaphragm and abutment and at the abutment/foundation interface (Steinberg, Sargand, and Bettinger, 2004). Longitudinal expansion/contraction of the bridge is taken in foundation and the bridge behaves similar to a frame.

In semi-integral bridges, the deck, girders, approach slab, and diaphragm act together as a single unit. Flexible bearing surfaces such as elastomeric pads are used in place of the bonded construction joints used for integral abutment bridges. A semi-integral bridge is illustrated in a side view (Figure) and section view (Figure). The flexible bearing surfaces provide more flexibility at diaphragm/abutment interface. Thus the magnitude of the forces transferred to the foundation is theoretically decreased (Steinberg, Sargand, and Bettinger, 2004). In order to prevent unwanted materials such as soil and aggregates from restraining the movement of the diaphragm/abutment joint

and diaphragm/wingwall joint, polystyrene is used to fill the joint's gap. The structural behavior of these types of bridges is affected by both the temperature changes and loading conditions imposed on the bridges.

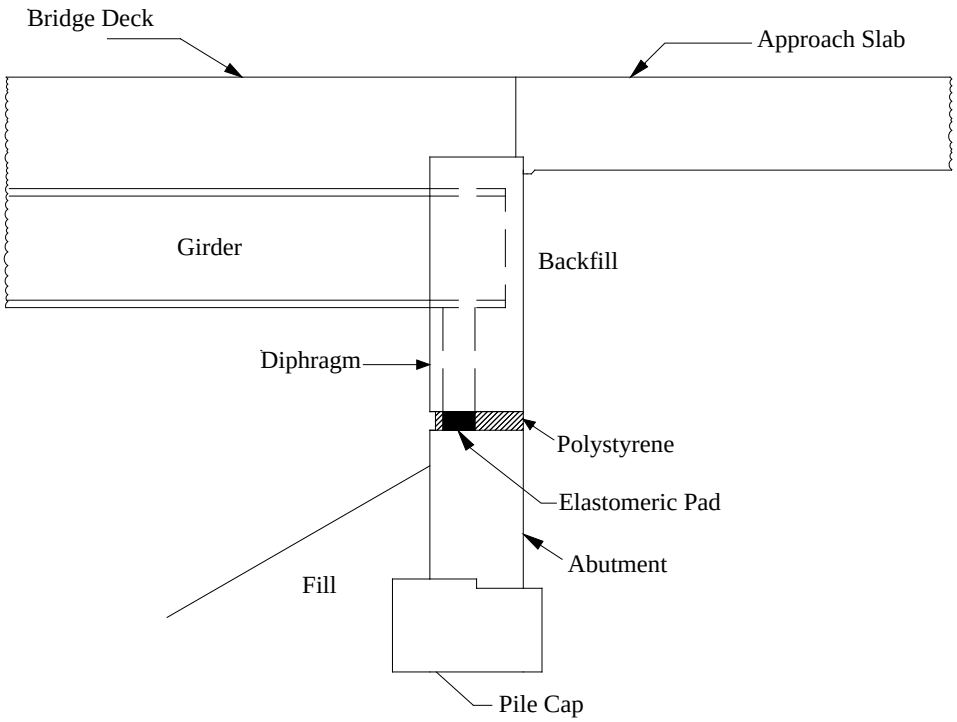

Figure 1: Semi-Integral Abutment and Diaphragm (Side)

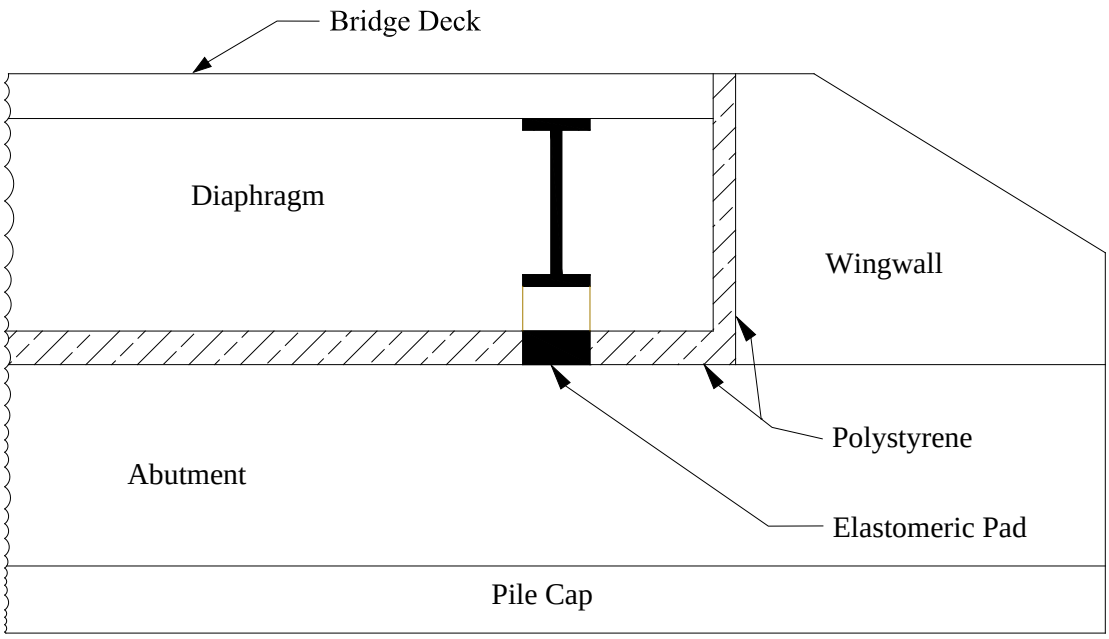

Figure 2: Semi-Integral Abutment and Diaphragm (Section)

It is known that bridges expand as they undergo an increase in temperature. This increase in temperature causes the bridge diaphragms to be pushed outwards and into the soil, which causes the soil pressure to be increased. The impact of the combined effect of the expansion of bridge coupled with the backfill soil pressures is still uncertain (Metzger, 1995). Prior research has also shown that skewed semi-integral bridges tend to rotate as the ambient air temperature increases through the season. One analysis showed that the superstructure of a skewed semi-integral bridge will tend to rotate in the horizontal plane unless otherwise retrained by guide bearings (Burke, 1994a). The magnitude of this rotation is greater for bridges with higher skews and occurs sooner for bridges with longer span length than those with shorter span length (Burke, 1994a). As a result of the bridge trying to rotate, forces are generated and transferred to the wingwalls of the bridge.

1.2 Purpose

ODOT does not currently have a procedure to determine the forces generated in the wingwalls from the thermal expansion and rotation of skewed semi-integral bridges. In a former

study, it was determined that these thermal forces can be significant. However, this study examined a bridge with a minor skew and wingwalls that were parallel to the diaphragm of the bridge. In addition, the instrumentation used to measure the forces was localized in a relatively small area of the wingwall and may not have provided a representation of the forces existing over the height of the wingwall. Larger skews and longer spans may produce even larger forces. The effects of the stiffness of the backfill behind the diaphragm and the approach slab on the magnitude of the forces transferred to the wingwalls is also not fully understood

Wingwalls that are parallel to the diaphragm of the bridge are subjected to an axial force from the thermal movement. ODOT is now utilizing more wingwalls that are turned back and run perpendicular or nearly perpendicular to the diaphragm. Wingwalls that are turned back would be subjected to bending from the thermal movement in addition to the axial force. Stresses from the combined bending and axial forces could be critical in the design of the wingwall.

1.3 Objectives

The main focus of this research project was to utilize the results of field assessments, as well as a computer analysis, in order to achieve the following:

- Evaluate conditions of wingwalls and wall abutments
- Asses the cause of the observed distress in the walls
- Monitor the movement of the bridges due to temperature changes
- Begin to develop guidelines to assist in achieving improved design of skewed semi-integral bridges
- Improve the understanding of the soil-structure interaction between superstructure, substructure, and embankment soil due to changes in temperature

To meet these objectives, the two skewed semi-integral bridges bridges were located in the northern and central Ohio were instrumented and analyzed in this project. In addition a parametric study was performed to assess other parameters affecting the bridge's behavior.

CHAPTER 2: LITERATURE REVIEW

The amount of research conducted on the design and behavior of skewed semi-integral bridges due to thermal expansion is very limited. As such, information pertaining to the effect it has on wingwalls and foundations is difficult to obtain. Substantial amount of research work however, has been done on the pressures and forces acting on the abutment of skewed integral bridges due to thermal expansion (Bettinger, 2001).

2.1 Burke

Martin P. Burke has documented his research work conducted on the longitudinal, lateral, and rotational movement of semi-integral bridges in several publications (Burke, 1994A.; Burke, 1994B; and Burke and Gloyd, 1994). His most recent publication summarizes previous work on semi-integral, as well as, integral bridge behavior (Burke, 2009). An insight on the behavior of skewed semi-integral bridges due to thermal expansion can be gained by making reference to Figure. In response to a rising temperature of the superstructure in a semi-integral bridge, an elongation (ΔL) is experienced by the bridge. The backfill in turn reacts to produce resistive compressive passive soil pressures on both diaphragms of the bridge. The resultant of these compressive passive soil pressures is denoted by P_P. Thus, a force P_E is developed in the bridge as a result of the expansion. The generated force P_E of a skewed semi-integral bridge with skew angle θ is resisted by the longitudinal component ($P_P \sec\theta$) of the resisting compressive passive force (P_P) of the soil being compressed behind the diaphragms. The lateral component ($P_P \tan\theta$) of the resisting passive force helps to resist the frictional backfill force ($P_P \tan\delta$).

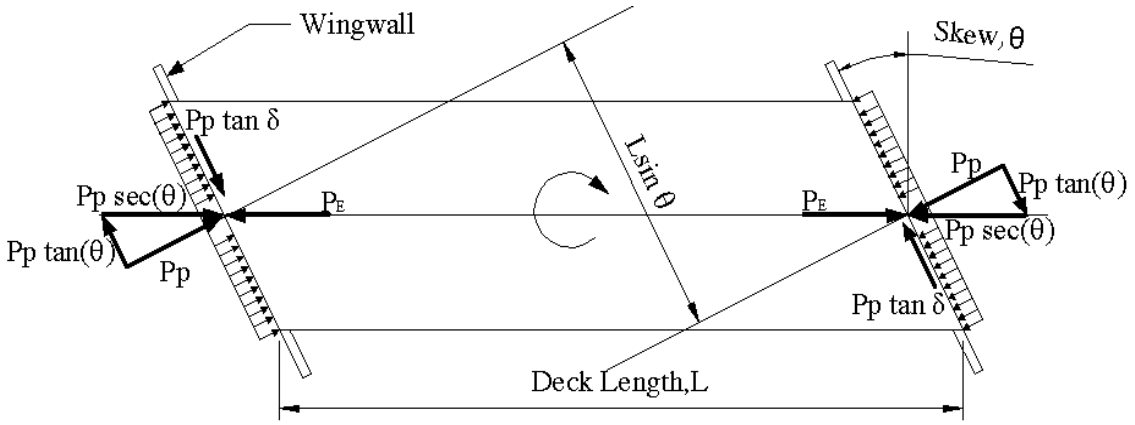

Figure 3: Horizontal Plane Rotation and Forces on Semi-integral Bridge

In skewed semi-integral bridges, Burke noted the resultant forces of the passive soil pressures developed at both ends of the bridge due to longitudinal expansion of the bridge are not concurrent. A moment couple is therefore produced from the non-concurrent forces that could potentially lead to the rotation of the bridge towards its acute corners in the manner shown in Figure. In order for the superstructure of a skewed semi-integral bridge to be stable, the force couple system that is causing rotation as described above must be resisted by an equivalent force couple system. This can be stated in Equation (1) as:

$$P_p L\sin\theta \leq P_p \tan\delta \; L\cos\theta \qquad (1)$$

where:

$P_p L\sin\theta$ = Force couple developed from the passive soil pressure behind the diaphragm

$P_p \tan\delta L\cos\theta$ = Frictional resistive between the diaphragm and soil force couple

Burke found that using reasonable values of a factor of safety of 1.5 and a 22^o angle of friction, δ, between the diaphragm/soil interface results in a stable system if the bridge's skew is $< 15^o$. For bridge skews larger than 15^o, rotation will likely be initiated

unless guide bearings are provided. In addition Burke has noted that once rotation is initiated, soil pressure behind the diaphragm will be increased at the bridge's obtuse corner and reduced at the acute corners. This will shift the resultant force from the soil pressures and reduce the force couple tending to cause the rotation. Therefore, rotational movements would be reduced during accompanying thermal cycles. However, the rotation would continue to produce cumulative effects until the movement is restrained by other means.

2.2 Steinberg, Sargand, and Bettinger

Field and analytical research related to skewed semi-integral bridges carried out by Steinberg, Sargand and Bettinger can be found in several references (Steinberg, Sargand, and Bettinger, 2004; Steinberg and Sargand, 2001; and Bettinger, 2001). This research was conducted to determine the forces exerted in the wingwalls of skewed semi-integral bridges in Athens County and Tuscarawas County, Ohio. The research was conducted with the aim of gaining a better understanding of the effect that changing ambient temperature has to the forces exerted on the wingwalls of skewed semi-integral bridges. The wingwall/abutment joints of two bridges in Ohio were instrumented to monitor the movement of the bridges as well as the forces generated in the wingwalls due to thermal expansion. The Tuscarawas County bridge had a single span length of 87ft and a roadway width of 32ft with a skew angle of 65^{o}. It was made up of composite reinforced concrete deck supported by steel girders. The backfill material for this bridge was sandy soil. The Athens County Bridge however, was a four span continuous steel

girder semi-integral bridge, also with a composite reinforced concrete deck. The outer and inner spans were 70ft and 87ft long, respectively. The roadway width was 40ft wide and the skew angle was 25^{o}.

In addition to the instrumentation of the bridges, computer analysis was carried out in order to validate the data collected in the field. SAP 2000 was used to model the Athens County bridge to determine the forces generated and exerted on the wingwalls. In addition, bridges were analyzed with multiple skew angles and span lengths in order to determine the impact a greater skew or longer span length has on the forces generated against the wingwalls.

The research discovered that significant wingwall force up to a maximum of 35.7 kips in magnitude was experienced by the Tuscarawas County bridge and up to a maximum of 30.1 kips in magnitude was experienced by the Athens County bridge during the course of the study. It should also be noted that the instrumentation to measure the forces was limited to a small area of the wingwall/diaphragm interface. The maximum longitudinal movement recorded for the Athens County bridge was 0.6442 in. and a maximum movement into the wingwall of 0.1295 in. was also measured. Based on the data recorded, direct correlation between the ambient temperature and the generated forces for the bridges did not exist or was limited. Nonlinear relationships existed between the wingwall/diaphragm interface joint movement and the force generated in the wingwall.

Analytical results revealed that as the bridge skew angle increases, so does the force generated in the wingwall. Also for a larger skew angle, the increase in the

wingwall force was higher as the backfill stiffness increased. Based on this work Equation (1) was modified to include the effects from the wingwalls as shown in Equation (2).

$$Pp\ L\sin\theta = Pp\ \tan\delta\ L\cos\theta + \text{(additional force couple from wingwalls)} \qquad (2)$$

2.3 Ohio Department of Transportation

With the principal goal of eliminating the bridge deck joints, designers in the state of Ohio adopted the design of continuous integral concrete bridges and continuous integral steel bridges which began over 6 decades and 3 decades ago, respectively (Burke, 1994B). There were however, few exceptions in the sense that joints were provided at the ends and center of bridges with span length longer than 600ft. In addition, bridges with a skew angle greater than 30^o, those longer than 300ft, curved bridges, and those with wall or stub abutments were also provided with joints. The inadequate functional quality and durability of the provided deck joint sealing systems and the constant maintenance associated with it caused designers in Ohio to innovate ways of combining the attributes of integral construction to those of bridges with movable joints (Burke, 1994B). As a consequence, the semi-integral bridge design concept was adopted. Prior to the development and adoption of semi-integral bridges, the application range of deck-jointed bridges was limited to 400ft span length with no skew or 200ft span length with a maximum skew angle of 30^o. With the introduction of semi-integral bridges however, the limits were expanded to the extents shown in Figure (Burke and Gloyd, 1994). Several characteristics outlined by Burke (1994b) need to be

recognized and provided for by design engineers. However, for the purpose of this thesis, only longitudinal, lateral and rotational restraint were discussed.

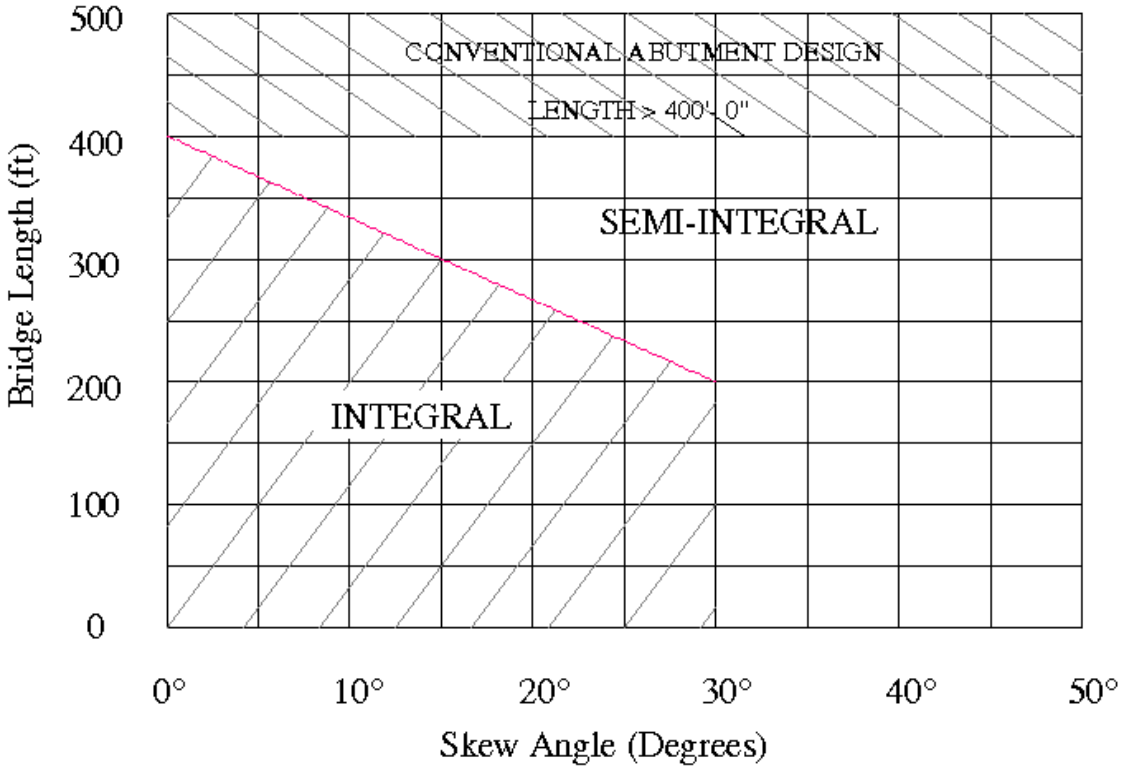

Figure 4: Abutment Type Limitations (Bridge Design Manual, 2007)

In the state of Ohio, wingwalls are currently designed to act only as retaining walls for the adjacent embankment soil (Bridge Design Manual, 2000). The forces exerted on the wingwalls by the superstructure due to thermal expansion are not considered. Wingwalls have typically cantilevered out from the bridge along the skew of the bridge (see Figure 5). However, wingwalls are recently being constructed more in a parallel alignment (turned back position) to the bridge longitudinal axis (see Figure 6). The parallel alignment (turned-back position) of the wingwall provides an additional

longitudinal restraint by way of backfill/wingwall friction or shearing resistance of backfill for wingwalls with rough surfaces due to the increase in confining pressure imposed by the turned back wingwalls (Burke, 1994B). However, it is important to note that the wingwall now becomes more subjected to bending stresses (Figure 6) than axial compression (Figure 5) from rotation of a skewed bridge.

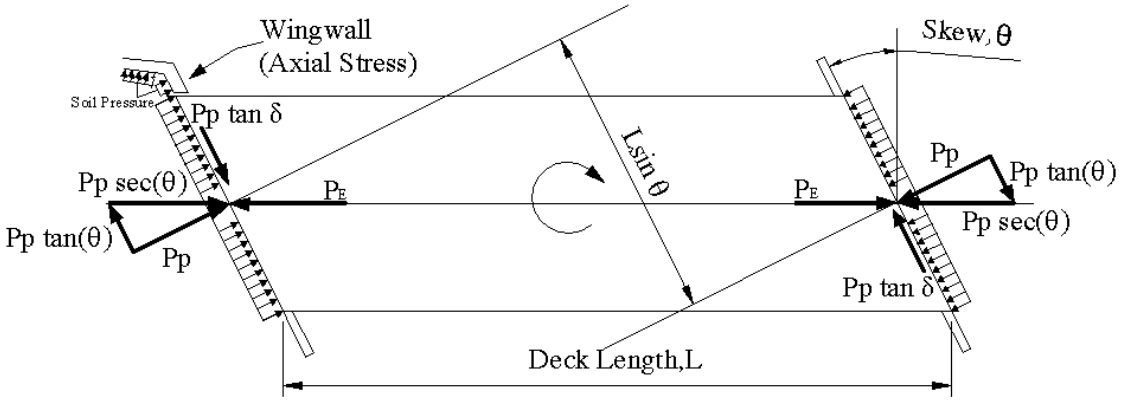

Figure 5: Typical Cantilevered Wingwall

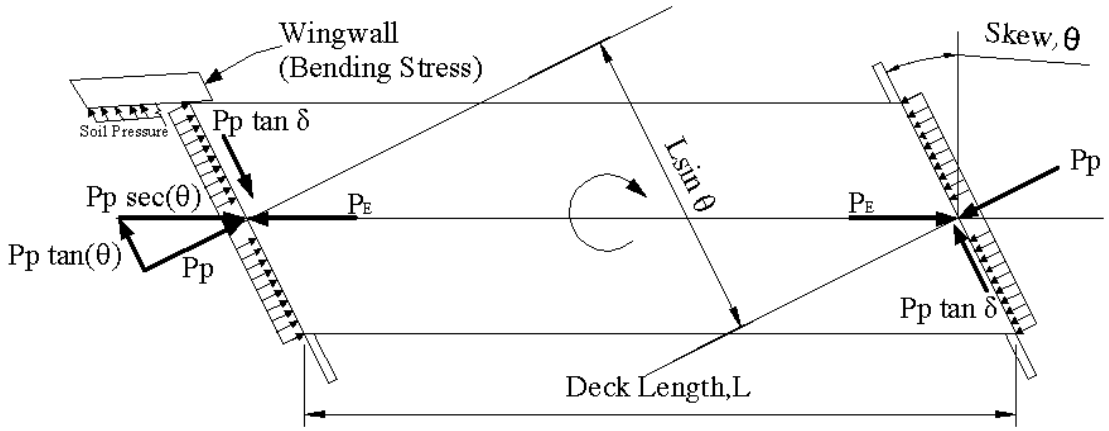

Figure 6: Parallel Aligned Wingwall

CHAPTER 3: FIELD EVALUATION

Part of the research in this project involved monitoring bridge in two different geographical locations in Ohio. One bridge was located in northeastern Ohio near the city of Defiance. The other bridge location was in central Ohio near the city of Newark. This chapter discusses the details of the bridges and the associated field evaluations.

3.1 Bridge Details

3.1.1 DEF-24-0981

This bridge location was on US-24 over the Tiffin River near Defiance, Ohio. Though two similar bridges exist at this location, only the westbound bridge was instrumented and studied. Construction began on the bridge in May 2006. The bridge is a four-span 440-foot composite structure with outside spans of 120 feet and inside spans of 100 feet. It has a skew of 45 degrees and features six 72-inch Modified AASHTO Type IV prestressed concrete I-beams. The roadway width is 42'-0" from toe-to-toe of the parapet wall barriers. The reinforced concrete deck is 8½" thick between girders and 10½" thick over the girders. The approach slabs are 30 feet long and 17 in. thick. The bridge's substructure includes semi-integral abutments and drilled shaft foundations. The wingwalls run parallel to the bridge. The wingwall at the acute corner of the rear abutment for the westbound bridge was instrumented. This wingwall was 18 in. thick, over 18 feet in length, and more than 8 feet high. Seismic pedestals exist at the piers but no guide bearings existed at the abutments.

The concrete for the instrumented wingwall was poured on November 29, 2006. Placement of the concrete for the deck and diaphragm was completed on May 18, 2007. The backfill behind the wingwall was placed in early June of 2007, and the approach slab was poured in late June of 2007. Bridge construction was completed and the two westbound lanes opened to the public in August 2007. Figure 7 shows the completed bridge.

Figure 7: DEF-24-0981

3.1.2 MUS-16-0261

This location actually consisted of two nearly identical bridges for east and west bound State Route 16 located in Muskingum County, Ohio. Both of these bridges were instrumented some time after their completion. The bridges were part of a project which involved the upgrading of a 2.36 mile stretch of S.R 16 (see

Figure 8) from a two lane to four lane highway. The bridges pass over Raiders Road and were opened to traffic in 1998.

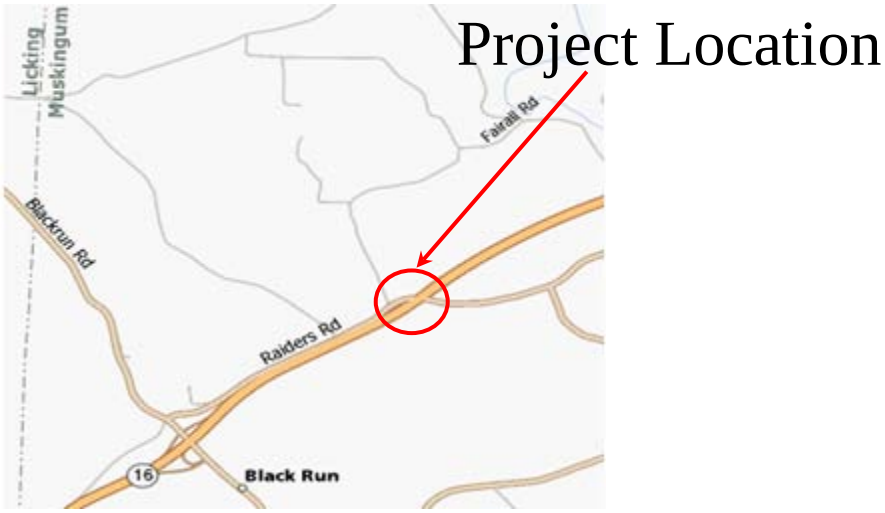

Figure 8: MUS-16-0261 Location

The east and west bound single span bridges have a total span length of 140ft and 139ft from center to center of bearing, respectively. The bridges are 42ft wide from toe to toe of barriers. They are both semi-integral bridges with a skew angle of 45°. The deck is 9 in. deep and is made of 4.5ksi reinforce concrete. Approach slabs on both ends of the bridge are 25ft long. Figure 9 shows the superstructure framing layout of the west bound bridge. The girder sections of the bridges are grade 50 ASTM A572 welded steel plate girders spaced 10ft apart.

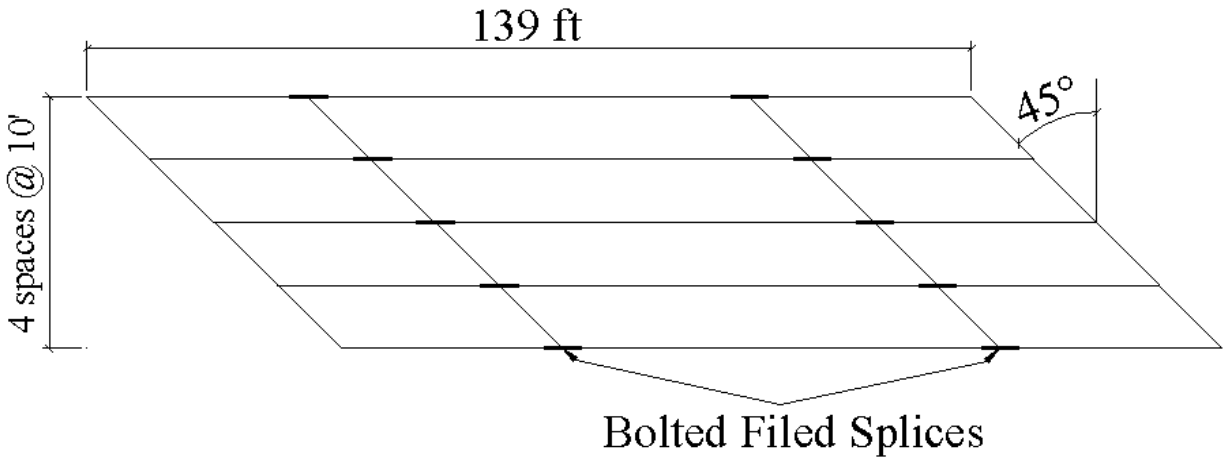

Figure 9: Superstructure Framing Layout (MUS-16-0261)

The girders are supported on short HP sections and bearing pads. The outside girders also have a bearing retainer assembly at the bearing pads to resist transverse movement of the girders. The bearing pads are supported by 19.1ft high wall abutments at each end of the bridge. As can be seen from Figure 10, the wall abutments are supported on a 3ft deep by 14.5ft wide 4 ksi concrete strip footing without any deep foundation. The wall abutments, which span the full width of the bridge, are tapered from 3ft at the top to 4 ft. at the bottom with the bridge span side of the wall being vertical.

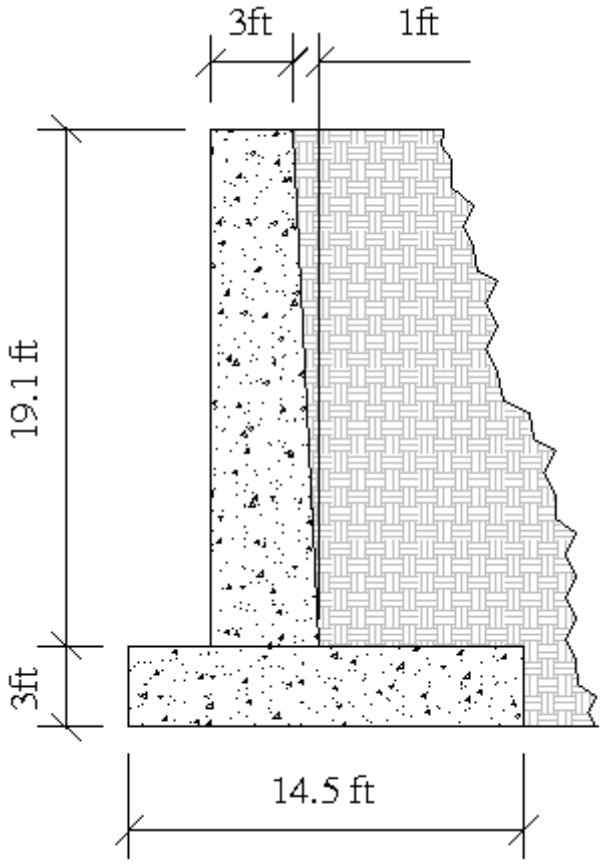

Figure 10: Abutment and Footing Section (MUS-16-0261)

After the bridge was open to traffic, signs of distress were observed as cracks at the abutment/wingwall interface of the west wall of the west bound bridge as well as the east wall of the east bound bridge. Pictures of the observed distresses are shown for the west wall (Figure 11) and the east wall (Figure 12), respectively. Initially, the cracks were patched but only proved to resurface again. Over time, the cracks were observed to have propagated as shown in Figure 13.

Figure 11: Observed Distress of West Wall (West Bound Bridge)

Figure 12: Observed Distress of East Wall (East Bound Bridge)

Figure 13: Propagated Cracks of West Wall (West Bound Bridge)

3.2 Instrumentation

3.2.1 DEF-24-0981

Two types of instrumentation were utilized for this bridge. Geokon Model VCE-4200 Vibrating Wire (VW) Strain Gages were used to measure both strain and temperature inside the wingwall. These VW strain gages are specifically designed for direct embedment in concrete. The Geokon VCE-4200 VW strain gage has a gage length of approximately 6 in (150 mm), a standard range of 3000 microstrains (με), a resolution of 1.0 με, and a temperature range of -68°F (-20°C) to 176°F (80°C). The VW strain gage is commonly used to measure strain in

foundations, piles, bridges, dams, and similar structures and utilize the vibrating wire principle to measure strain. This principle involves a length of steel wire is tensioned between the two end blocks of the gage, which is directly embedded in concrete. Deformations, or strain changes, inside the concrete structure causes the two end blocks to move relative to one another. These changes in strain affect the amount of tension held in the steel wire. This tension is then measured by electronically plucking the wire and measuring its resonant frequency of vibration with the use of an electromagnetic coil inside the gage. The vibrating wire strain gages are primarily designed for long-term strain measurement and thus are not suitable for measuring dynamic strains. The gages are also fully waterproof. Figure 14 depicts one of these strain gages along with its connected wiring which allows for measurement of both strain and resistance in the vibrating wire contained in the gage.

Figure 14: Geokon Model VCE-4200 Vibrating Wire Strain Gage

Strain gage instrumentation took place after reinforcing steel was placed in the wingwall but before the concrete was poured. Vibrating wire strain gages were attached to the wingwall reinforcing bars with the use of steel wire and duct tape in a manner such that the installation

allowed strain measurements within the concrete. Figures 15 and 16 show the installation of the VW strain gages in the wingwall.

Figure 15: Vibrating Wire Strain Gage Installation

Figure 16: Vibrating Wire Strain Gage Tied to Reinforcement

A total of eight VW strain gages were installed in the wingwall. All of the gages were oriented perpendicular to the face of the wingwall in order to measure the strains placed on the wingwall as a result of thermal expansion and contraction of the bridge. As seen by the plywood form in Figure 16, the gages were all placed approximately 1" from the edge of the wingwall nearest the diaphragm. The eight VW strain gages were placed in two columns of four gages. One column of gages were installed as close as possible toward the bridge and other column of gages was closer to the approach slab. The locations of the gages in relation to each other have also been are shown in Figure 17. Although not noted in the diagram, the top of the wingwall is located at a height of approximately 8'3" above the base. The vibrating wire strain gages were labeled based on their location with respect to height and to which end of the bridge each was closest. The left column of four gages was designated the soil (S) side, whereas the four right-hand gages were labeled as bridge (B) side gages. The labeling with respect to elevation (TOP, MIDT, MIDB, and BOT) can also be seen in Figure 17. The installation of VW

strain gages was completed in November 2006, and the concrete for the wingwall was poured the following week.

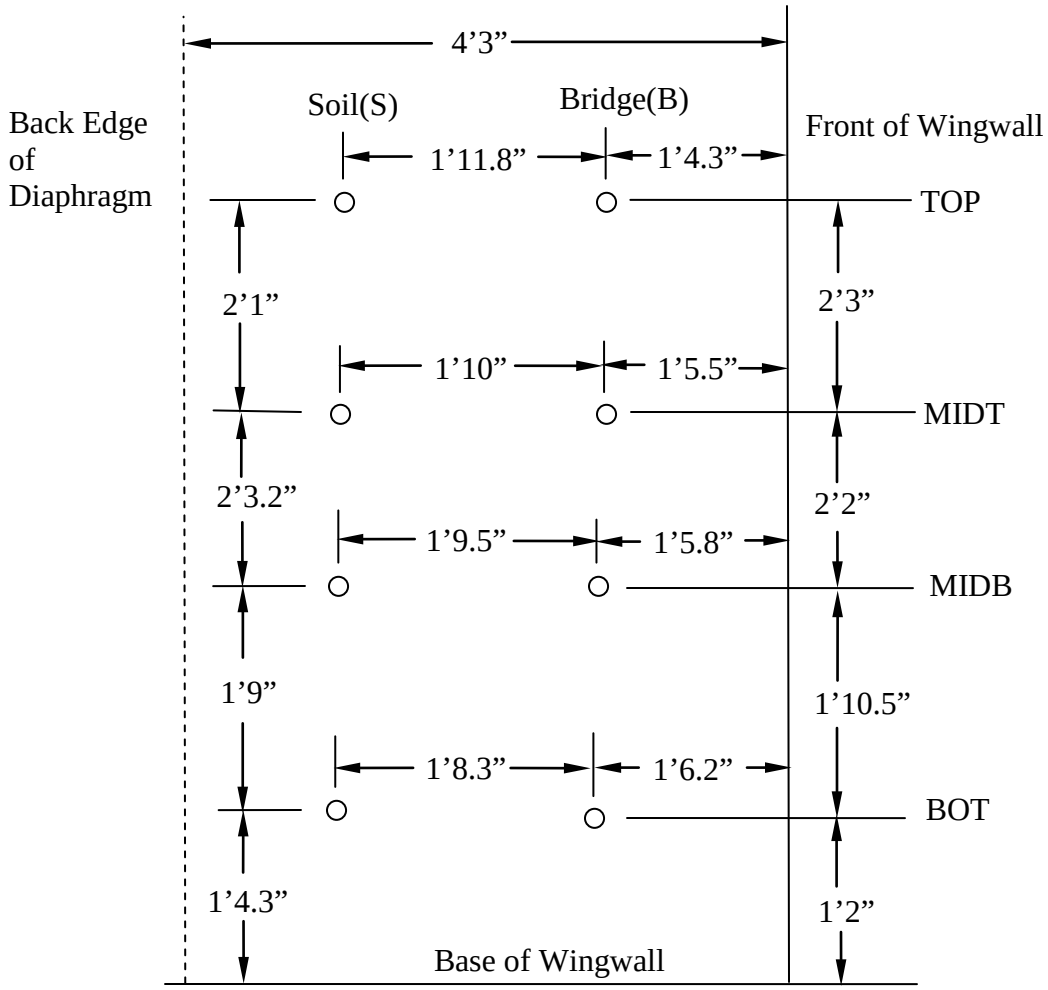

Figure 17: Vibrating Wire Strain Gage Locations

Strain measurements of the vibrating wire strain gages were taken using a Geokon Model GK-401 Microprocessor as shown in Figure 18. The measurement output was in units of microstrain. However, the strain has to be corrected for temperature in order to account for the strain only due to loading. The corrections are necessary due to slight differences in the thermal coefficients of the gages and the concrete. Equation (3) was used to determine the strain from loading.

$$\varepsilon = (R_1-R_0)\,B + (T_1-T_0)\,(C_1-C_2) \qquad (3)$$

where

ε = the strain due to load

R_1 = strain reading

R_0 = initial strain reading

B = batch calibration factor for gage

T_1 = temperature

T_0 = initial temperature

C_1 = thermal coefficient for steel (gage)

C_2 = thermal coefficient for concrete

The difficulty with using Equation (3) is that the thermal coefficient for concrete has a fairly large range and could vary with location within the wingwall. Based on the VW strain gage manufacture's recommendation, a value of 12.2 microstrain/^{o}C was used for the thermal coefficient of the gage. Several values were investigated based on the data for the concrete and a final value of 11.3 microstrain/^{o}C was used for the thermal coefficient of the concrete.

In addition, temperature measurements of the VW strain gages were taken with the use of a Fluke 87 Series III True RMS Multimeter as shown in Figure 19. Using the green and white lead wires of the strain gages, a resistance reading in units of kilo-ohms (kΩ) was measured. The resistance reading was then converted to a temperature in degrees Celsius (°C) by using the formula shown in Equation (4).

$$T = 1/\,[A + B(\ln R) + C(\ln R)^3 - 273.2] \qquad (4)$$

where

T = temperature in Celsius

ln R = natural log of thermistor resistance in Ω

A = constant of 1.02569×10^{-3}

B= constant of 2.478265×10^{-4}

C = constant of 1.289498×10^{-7}

The formula in Equation (4) was provided in the specifications for the Geokon Model VCE-4200 Vibrating Wire Strain Gages. Finally, the Celsius temperature was then converted to degrees Fahrenheit (°F) using Equation (5).

$$T_{°F} = 1.8\ T_{°C} + 32°F \qquad (5)$$

where

$T_{°F}$ = temperature in degrees Fahrenheit

$T_{°C}$ = temperature in degrees Celsius

Figure 18: Geokon Model GK-401 Microprocessor

Figure 19: Fluke 87 Series III True RMS Multimeter

In addition to the VW strain gages, digimatic indicator targets were used to monitor the expansion and contraction of the joint between the diaphragm and wingwall. The 1 ½" long stainless steel targets were permanently embedded in the concrete, while the 5/8" steel screws are threaded into the targets in order to take measurements. By using the embedded targets, the digimatic indicator is able to measure movement towards and away from the wingwall at a high accuracy. Installation of the digimatic indicator targets originally occurred on the top surface of the wingwall and diaphragm soon after the concrete was poured. However, due to the placement of a parapet wall in the location of these targets, new targets had to be installed in late August of 2007 at the vertical face of the wingwall-diaphragm interface. The digimatic indicator targets are located on each side of the expansion joint material between the wingwall and diaphragm. A diagram of the targets and their labeling can be seen in Figure 20. Target rows two and three were the original two locations of the targets. However, due to the limited range of the digimatic indicator device, rows one and four were installed in October 2007 in order to properly take readings with the indicator.

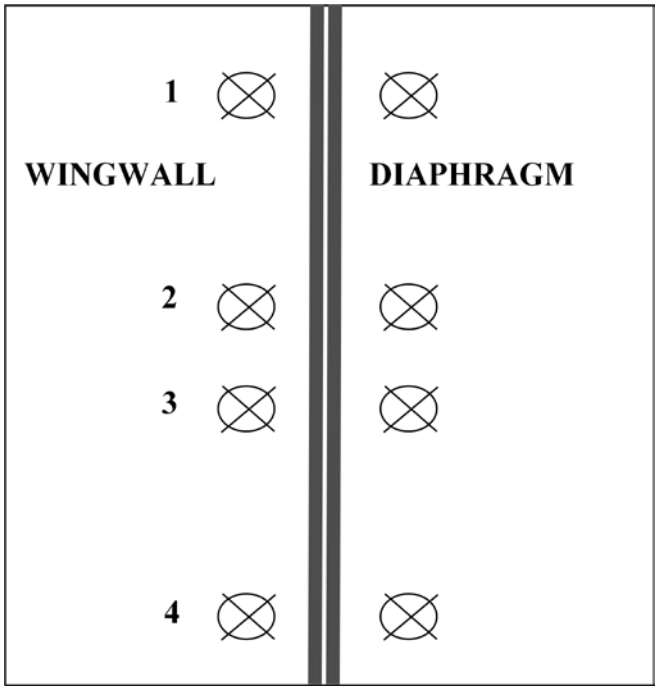

Figure 20: Digimatic Indicator Targets Location

The digimatic indicator target readings were taken with a Mitutoyo Model IDC112T ABSOLUTE Digimatic Indicator (see Figure 21). The indicator has a range of ±0.5 inches and an accuracy of 0.00012 inches. Readings were taken as a digital readout of four decimal places. In addition, one of the contact points on the indicator can be adjusted so that five different 0.5 inch ranges between approximately 1.7 and 10.24 inches can be used. Each time this contact point was moved, the steel calibration plate shown in Figure 22 was used to calibrate the digimatic indicator to the proper range for data collection.

Figure 21: Top view of Mitutoyo Model IDC112T ABSOLUTE Digimatic Indicator

Figure 22: Calibration Plate with Metal Targets

3.2.2 MUS-16-0261

These particular bridges were instrumented because of the signs of distress they displayed and the uniqueness of their abutment walls on a shallow foundation. It should also be noted that instrumentation was installed long after construction was completed negating internal sensors from being installed and resulting in difficulties of interpreting data. The wingwalls of the outside acute corners of both of bridges were instrumented because they showed signs of distress and wingwalls did not exist on the acute corners between the bridges due to the continuous abutment walls between the bridges. The wall abutments near the instrumented wingwall/diaphragm interfaces were also instrumented to monitor their tilt which was suspected to be due to either differential settlement and/or thermal effects. Thermal were installed to measure internal temperatures. A plan view of the instrumentation can be seen in Figure23 and 24.

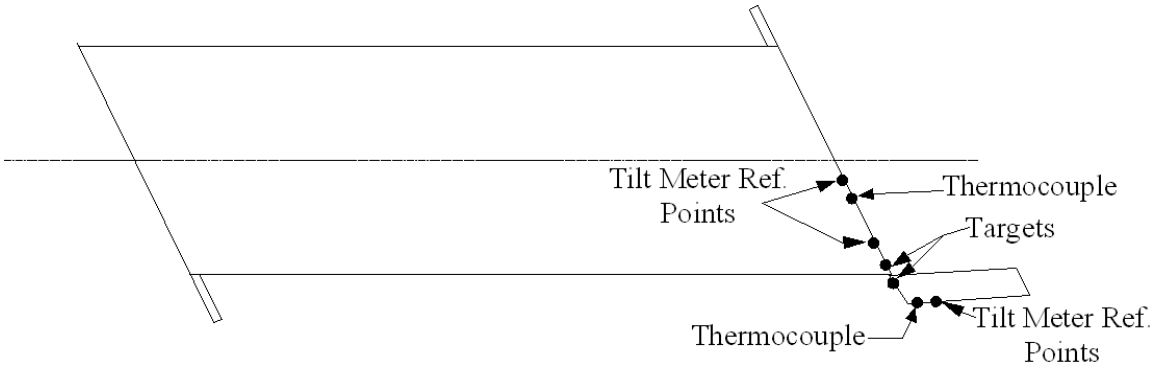

Figure 23: Instrumentation (East Bound Bridge)

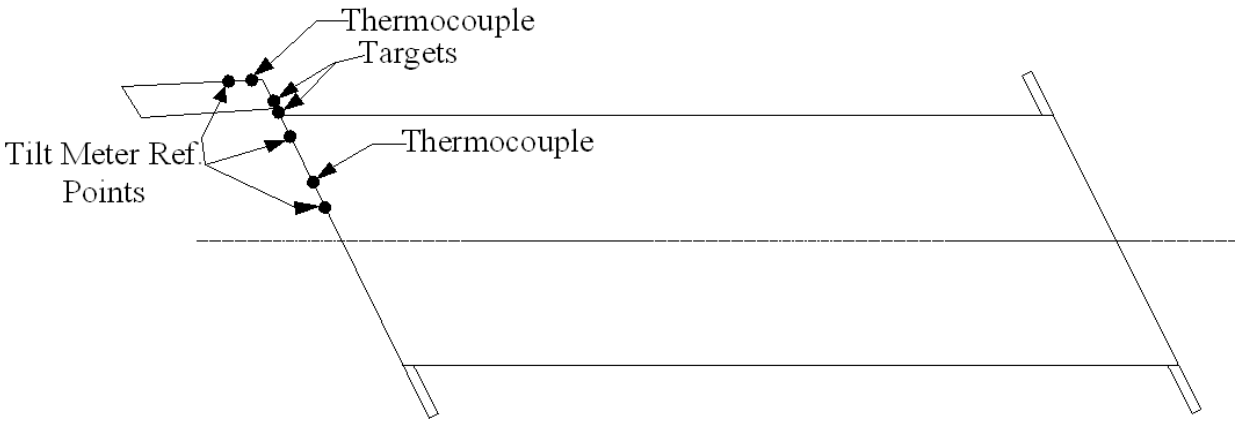

Figure 24: Instrumentation (West Bound Bridge)

The outside acute corners were instrumented to determine the effect thermal expansion/contraction of the bridges had on the wingwall/diaphragm interface joint. Digimatic indicator metal targets (see Figure 22) were installed on the walls of the bridges on each side of the wingwall/diaphragm interface joint. To install the metal targets, the desired distance between the two targets was measured, and holes were drilled at those locations. The concrete particles from the drilling were cleaned out of the holes to ensure a strong bond between the metal targets

and the concrete. The targets were then embedded into the walls and held in place with the use of a rapid setting two part epoxy. For the east bound bridge, two sets of targets were installed 8in and 10in apart, while on the west bound bridge only one set of targets installed 8in apart was used. Figures 25 and 26 show the approximate locations of the targets. The installation of the west bound bridge metal targets was done several months after the initial installment of instrumentation due to difficulties in gaining access to the height of the desired location. In addition to that, the topography of the ground surface adjacent to the location at which the installation was to take place was very steep and considered dangerous for the installation crew.

Figure 25: Target Location (East Bound Bridge)

Figure 26: Target Location (West Bound Bridge)

The expansion and contraction measurements were taken with the Mitutoyo Model IDC112T ABSOLUTE Digimatic Indicator (see Figure 21). Prior to any measurements, the Digimatic Indicator was calibrated to the appropriate target spacing, 8in or 10in. A decrease in the pre-set gauge length indicated expansion of the bridge while an increase in the gauge length indicated contraction of the bridge.

The measuring of the angle of tilt for the wingwalls and abutments was attained by establishing measurement stations on the bridges. A total of six stations were set up with three stations on each bridge. Figures 27 and 28 show the locations at which the stations were established on the walls of each bridge. The reference points circled in black with the arrow

pointing to the left were located further to the left in the picture. For each bridge, one station was established on the wingwall and the other two were established on the wall abutments.

Figure 27: Tilt Reference Stations (East Bound Bridge)

Figure 28: Tilt Reference Stations (West Bound Bridge)

In order to establish a reference station, a rebar locator was used to determine the location of the rebars in the walls. This was done in order to assure availability of depth into the walls up to 2 in., as well as to prevent drilling into the rebars and possibly decreasing the structural integrity of the wingwalls or wall abutments. A vertical distance of 2.5 ft. was measured between the two points at which holes were drilled. The concrete particles were cleared after drilling to establish proper bond between the concrete and the stainless steel reference points. Using a quick setting two-part epoxy, two stainless steel reference points were embedded 2 in. into the concrete wingwall or wall abutment at each station.

The Digi-Tilt tiltmeter manufactured by Slope Indicator (Seattle, Washington) was used in the tilt measurements. The system comprises of a accelerometer sensor and a digital readout device. In order to take a tilt reading at a given measuring station, a stainless steel ball on a threaded shaft was screwed into each of the established reference points. A reference plate was

then positioned and held against the steel joints, and with the use of an accelerometer, readings were taken. The field set up for the data acquisition is illustrated in Figure 29. In addition, Figure 30 shows the components of the data acquisition equipment (readout device and accelerometer) while Figure 31 shows the reference plate hanging on the wall.

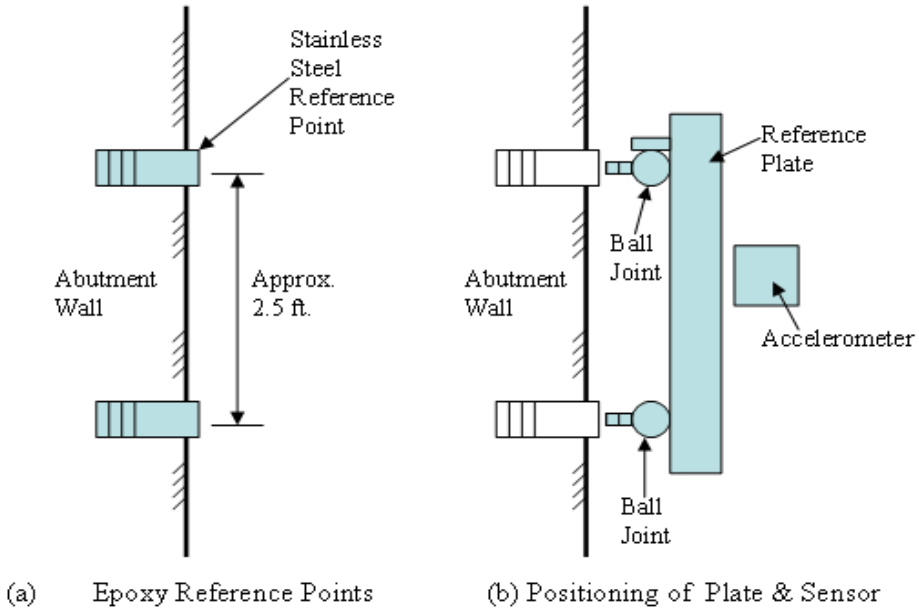

Figure 29: Field Set-Up for Data Acquisition (Masada, 2007)

Figure 30: Digi-tilt Sensor and Readout Device (Masada, 2007)

Figure 31: Reference Plate on Wall Abutment (Masada, 2007)

According to Masada (2007), the tilt-meter sensor has a range from -30^{o} to +30^{o} and a sensitivity of 0.003^{o}. One single measurement using the device consisted of two different readings, a positive and negative reading. In order to calculate the angle of tilt (θ) of the walls from the true vertical, the positive and negative readings obtained in the field were applied Equation (5) below.

$$\theta(rad.) = \sin^{-1}\left[\frac{(+\text{Re}ading)-(-\text{Re}ading)}{4}\right] \quad (5)$$

A positive θ value indicates that the wall tilted away from the backfill behind it, whereas a negative θ value indicated that the wall tilted into the backfill. It should be noted that the movement is based on an initial reading taken at the completion of the instrumentation since the bridge was constructed long before the reference points were installed.

In order to take the internal temperatures of the wingwalls and wall abutments, Omega type T (Copper – Copper-Nickel) thermocouples were embedded into the walls. These thermocouples have a maximum temperature range of -270 to 400^{o}C (-454 to 752^{o}F) and a tolerance of 1.0^{o}C (Omega Engineering, 2006). A total of two thermocouples were installed each on the west and east bound bridges. One thermocouple was embedded approximately 1 ½" on each wingwall and wall abutment and were both held in place using epoxy. A Digital Strain meter (TC-21k model 232) was used to record the temperature readings (see Figure 32). Different locations were used to determine if thermal variations existed between the wall abutments and wingwall.

Figure 32: Digital Strain Meter

3.2 Field Data

This section provides and discusses the data obtained from the instrumentation that was installed in and on the bridges.

3.1.1 DEF-24-0981

The data obtained from the instrumentation installed on DEF-24-0981 as seasonal temperatures changed is summarized in this section. Data obtained during field visits was stored electronically and processed with the use of spreadsheets. The strains from the VW strain gages were converted into stresses by multiplying the strains from the VW strain gages by the modulus of elasticity of the concrete. The modulus of elasticity for the wingwall was determined through typical standard computations from the average compressive strength of cylinders for the wingwall as provided by ODOT. The average compressive strength of the concrete was 5,095 psi. This resulted in an estimated modulus of elasticity of 4.07×10^6 psi when using the simplified normal concrete weight equation of $57{,}000 \sqrt{f'c}$. Compressive stresses were taken as negative.

Table 1 provides the average stresses from the VW strain gages along with the average internal and ambient temperatures. The average stresses are, in general, 100 psi or less. It is also interesting to note that the internal temperatures do not show as large a variation as the ambient temperatures.

Table 1: Average Stresses and Temperatures

	2007							2008						2009
	6/1	6/18	7/2	7/26	10/2	10/11	11/16	1/3	3/14	4/23	6/26	9/04	12/15	7/24
Avg Stress (psi)	-79	-108	-111	-113	-100	-104	-49	1	27	-5	-49	-88	-73	-93
Internal Temp (^{o}F)	82	87	71	73	-	62	44	28	41	61	-	78	36	71
Ambient Temp (^{o}F)	82	95	75	73	65	48	35	14	50	70	68	84	18	81

Figure 33 provides the average stress for the wingwall from all the VW strain gages compared to the average measured internal temperature. In general, an increase in temperature leads to higher average stress in the wingwall as expected. The data points at the same average temperature with different average stress are likely due to the complex behavior of the system from the thermal cycling. The maximum average stress reaches approximately 115 psi at a temperature of approximately 90^{o}F.

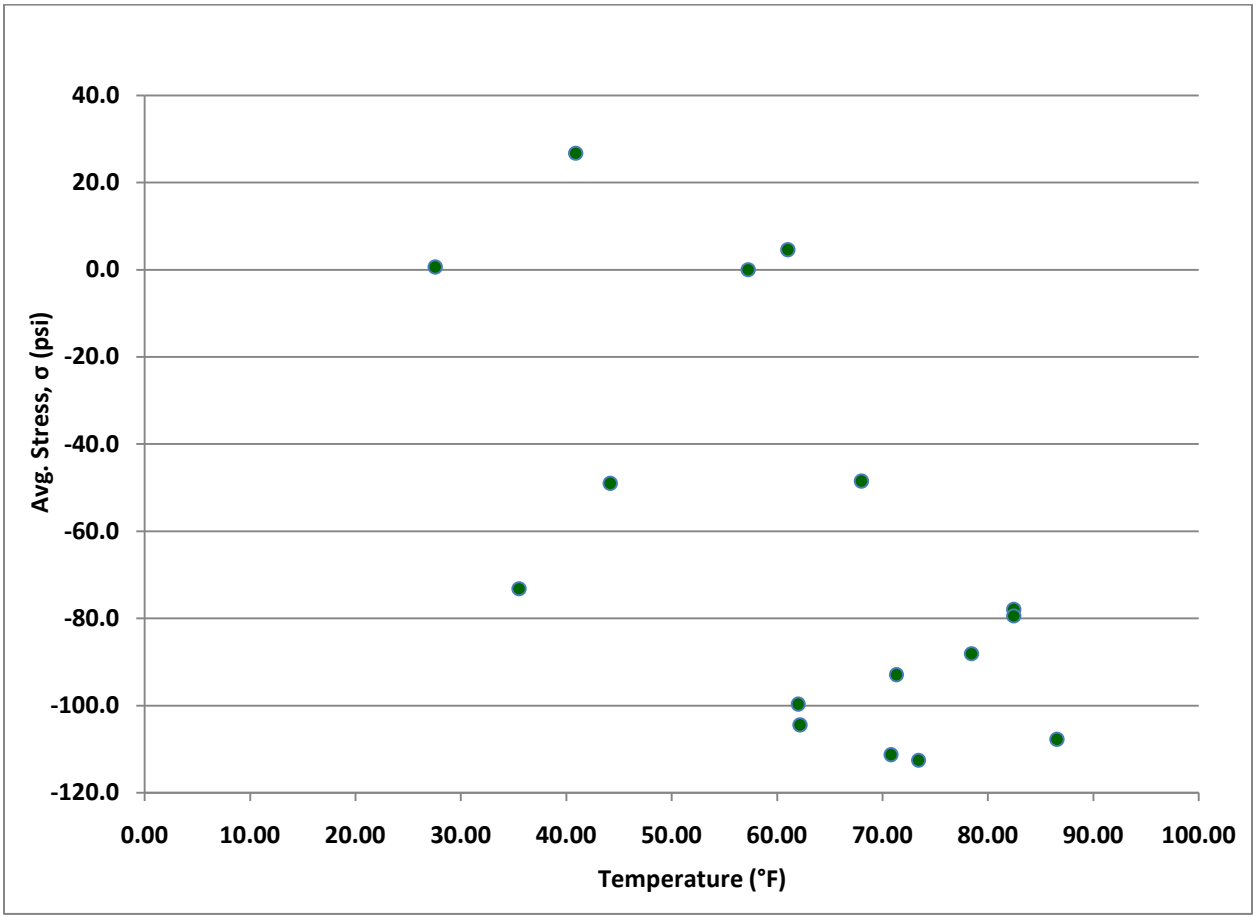

Figure 33: Average Wingwall Stress vs Average Internal Temperature (DEF-24-0981)

Graphs of the stress over the height of the wingwall measured from the VW strain gages are plotted in Figures 34-36. Legends are not provided in the graphs because of the large number of data sets. Figure 34 provides the data for the column of gages closest to soil side of the diaphragm (S gages) while Figure 35 provides the data for the column of gages closest to bridge side of the diaphragm (B gages). Figure 36 provides the average stress from the two VW strain gages at each of the four approximate gage heights. The gage locations were previously shown in Figure 17. The lines shown in Figures 34- 36 provide general shapes of the stresses over the height of the wingwall. The solid line depicts the general shape of the stress distribution from the initial construction of the wingwall until the following winter when the temperatures dropped and the bridge contracted. The data set for the solid line was taken on June 18, 2007 when the

average internal temperature from all the VW strain gages was 86^{o}F. This date was after backfill was placed behind the wingwall, but prior pouring of the approach slab. The shape of the solid line for the S gages (Figure 34) shows a relatively uniform stress distribution in the lower portion of the wingwall along with a decrease in stress near the top. For the B gages, the solid line depicting the stress distribution is almost linearly throughout the height of the wingwall (see Figure 35). The average stress distribution of both the S and B gages as shown by the solid line in Figure 36 is nearly uniform with a decrease for the upper portion of the wall.

Upon increases in temperatures in the spring of 2008, the general shape of the stress distribution over the wingwall height then changes into a shape depicted by the broken line (Figures 34-36). The data set for the broken line was taken on September 4 of 2008, slightly over a year after the bridge was open to traffic. The average internal temperature from the VW strain gages was 78^{o}F for the data set depicted by the broken line. The broken line depicting the stress distribution for the S gages (Figure 34), B gages (Figure 35), and the average of all gages (Figure 36) shows higher stress near 5.5' above the face of the wall with lower stress existing near the top and base of the wingwall.

For each of the two general stress distributions, the data sets at higher temperatures produce higher compressive stresses, as expected. In addition, the average stress over the height of the wingwall was always larger for S gages than the B gages. This is likely due to the rotational effects causing higher magnitude compression at the back of the diaphragm/wingwall interface compared to the front (bridge) side of the diaphragm/wingwall interface. The majority of stresses for the S gages are 150 psi or less with a few readings showing magnitudes as high as 200 psi. The majority of stresses determined from the B gages are 100 psi or less with a few readings exceeding 150 psi. The majority of the average stress readings on the wingwall based on the VW strain gages are less than 150 psi.

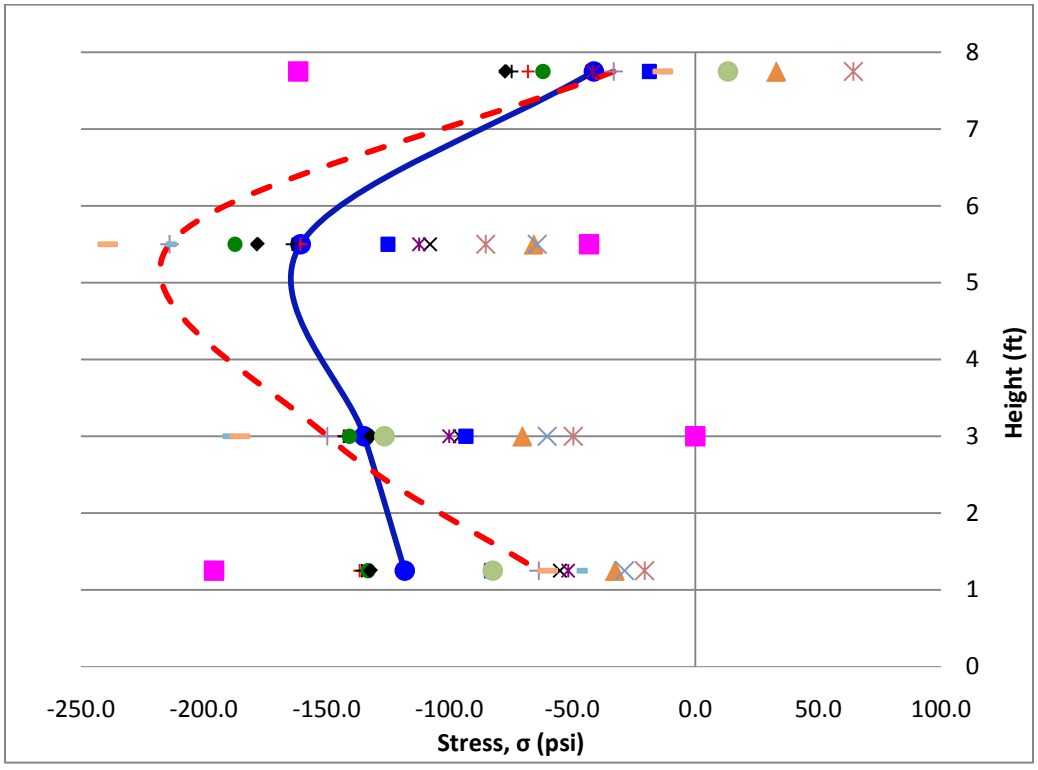

Figure 34: Wingwall Stress – S Gages (DEF-24-0981)

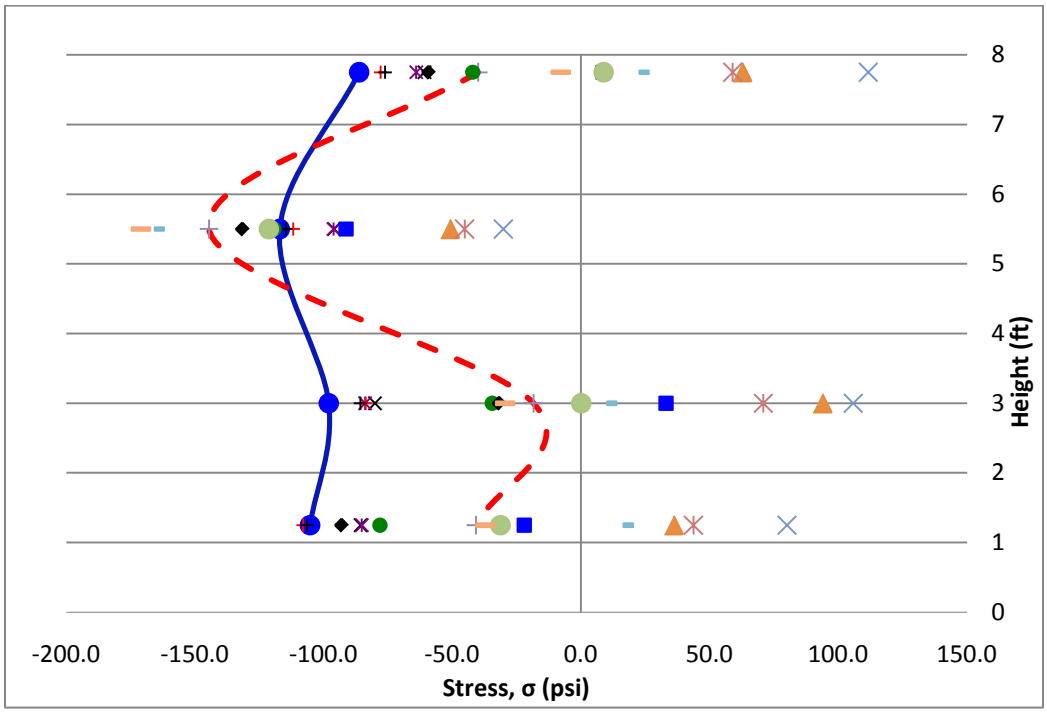

Figure 35: Wingwall Stress – B Gages (DEF-24-0981)

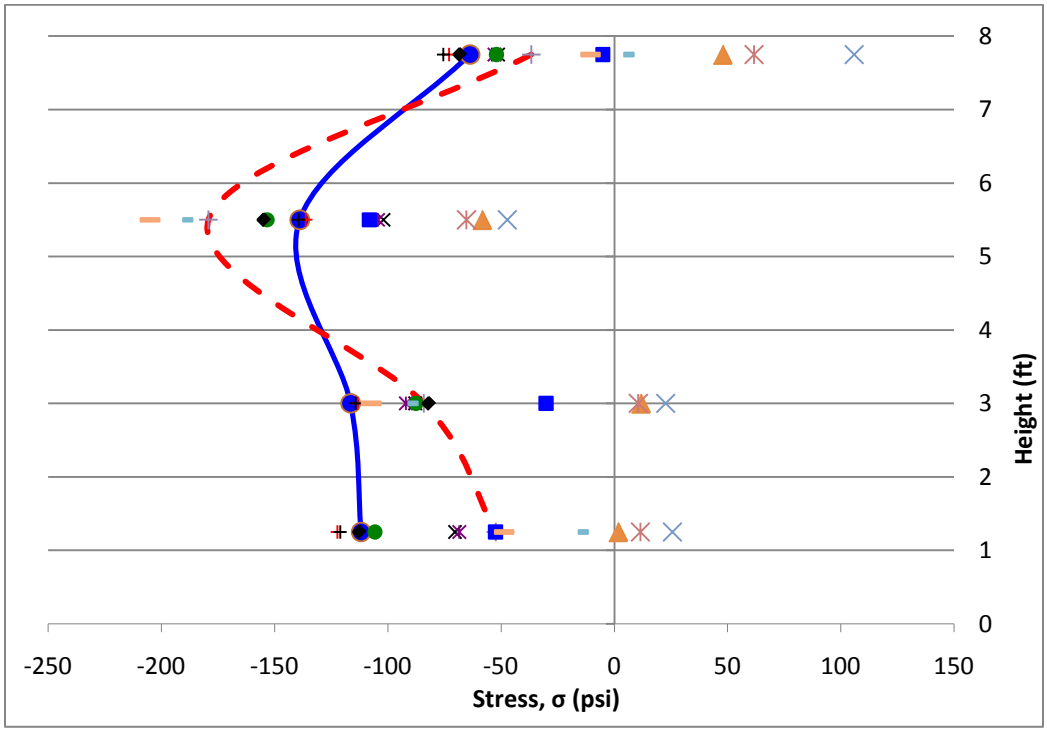

Figure 36: Average Wingwall Stress (DEF-24-0981)

The data from the digimatic indicator targets is provided in Table 2. A diagram of the targets and their labeling was previously shown in Figure 20. Recall target rows 2 and 3 were the original two locations of the targets installed in late August of 2007. However, due to the limited range of the digimatic indicator device, rows 1 and 4 were installed in October 2007 in order to properly take readings with the indicator. If distances between targets could not be measured with the indicator, a standard tape measure was used to obtain less accurate data. Table 2 provides the data to two decimal places even though the indicator provided accuracy to four decimal places. Table 2 also shows, in parenthesis beneath the data, the change in readings from the initial target readings. Positive changes are opening of the joint and negative readings are closing of the joint. The final row of Table 2 provides the average stress in psi recorded by the VW strain gages. When comparing target rows 2 and 3 with the average stress, it can be seen the opening of the joint corresponds with a lowering of the average stress. However, the magnitude of the joint opening is not consistent with stress values. For example, the largest opening of the joint on 1/3/2008 does not correspond with the lowest stress and the relatively

smallest opening on 6/26/2008 does not correspond to the highest stress near the initial reading stress. Finally when comparing the target readings from rows 1 and 4 with the average stresses, a trend is not clear. Though the stress dissipates with opening of the joint, the first sign of closing the joint on 3/14/2008 results in a stress much less than the initial stress for the target rows. The results of comparing the stress and the joint target readings show the complex behavior of the system.

Table 2: Digimatic Target Readings (DEF-24-0981)

Target Row	2007				2008						2009
	7/26	10/2	10/11	11/16	1/3	3/14	4/23	6/26	9/04	12/15	7/24
2	7.81	8.38* (0.56)	8.56* (0.75)	— —	10.00* (2.19)	8.56* (0.75)	8.24 (0.43)	8.20 (0.39)	8.24 (0.43)	9.00* (1.19)	8.38* (0.56)
3	7.96	8.19 (0.23)	8.38* (0.41)	— —	9.88* (1.91)	8.44* (0.47)	8.11 (0.14)	8.05 (0.08)	8.14 (0.17)	8.88* (0.91)	7.81 (-0.16)
1	— —	— —	9.81 —	10.04 (0.24)	10.24 (0.43)	9.80 (-0.01)	9.50* (-0.31)	9.38* (-0.43)	9.56* (-0.25)	10.23 (0.43)	9.62* (-0.18)
4	— —	— —	9.96 —	10.20 (0.24)	10.44 (0.48)	9.94 (-0.02)	9.62* (-0.34)	9.50* (-0.46)	10.62* (0.66)	10.38 (0.41)	9.69* (-0.27)
Avg Stress (psi)	-113	-100	-104	-49	-1	27	-5	-49	-88	-73	-93

*Data obtained with a tape measure

Figure 37 provides plots of the wingwall/diaphragm interface gap determined from the digimatic target readings compared to the average stress determined from the VW strain gages. The sequence of the data shown in Figure 37 is counterclockwise starting from the lower left. As expected, the stress deceases as the gap increases (1 in Figure 37). However at the top of the curves (2 in Figure 37), the gap decreases across all target rows with a decrease in stress. This is followed by a gap decease and stress increase with a similar slope to that of the first major gap increase and stress decease (3 in Figure 37). This is then followed by a large average stress increase with little change in the gap (4 in Figure 37). The gap then again changes little with another stress increase with the exception of target line 4 that shows a gap increase (5 in Figure 37). The final behavior of the gap and average stress (6 in Figure 37) shows typical behavior of

gap increases with stress deceases and then a final gap decrease with a stress increase. The graph of target line 3 actually follows along the same slope for this last stage. Target line 1 and 2 have slightly different slopes, but are relatively close for this last stage. The slopes of the curves are more shallow for this stage compared to stages 1 and 3 for all target lines. Target line 4 also returns to the decreasing gap and increase stress behavior that is expected in this final 6th stage compared to stage 5.

The unexpected behavior of the gap compared to the stress in a few of the stages may be due to the complex behavior exhibited at the wingwall/diaphragm interface caused by the thermal changes. The movement of the bridge's diaphragm at the interface is likely a combination of longitudinal sliding, movement in the direction of the skew into the wingwall, and rotation. This complex movement cannot be fully measured with the instrumentation installed only on the front face the wingwall/diaphragm interface.

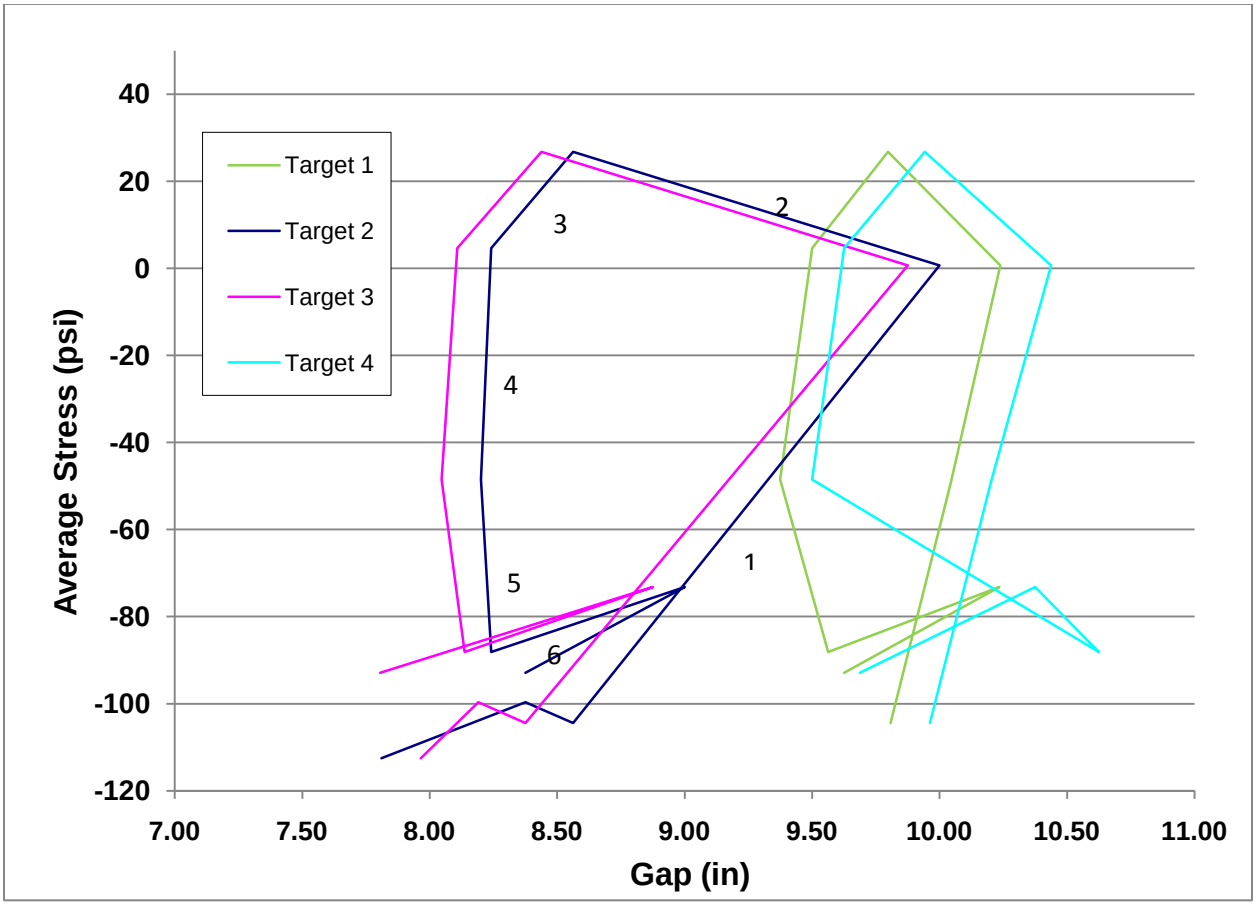

Figure 37: Interface Gap vs Average Wingwall Stress (DEF-24-0981)

Figure 38 provides graphs of the digimatic target readings compared to the average temperature of the wingwall from the VW strain gages. The sequence of the data shown in Figure 37 is clockwise starting from the upper left. As expected, the gap increases as the temperature decreases (1 in Figure 38). The bottom portion of the curves (2 in Figure 38), the gap decreases across all target rows with an increase in temperature. The slope of the curves for this stage is not as steep as that of the stage 1. The curves continue with the gap decreasing as the temperature rises (3 in Figure 38). For target lines 1 and 4, the slopes of the curves for this stage, 3, are similar to stage 1. Target lines 2 and 3 have slightly steeper slopes for stage 3 compared to stage 1. The curves for target lines 1-3 then show a minimal change in the gap with an increase in the temperature (4 in Figure 38). Target line 4 shows an unusual increase in the gap with a temperature increase. The final behavior of the gap and average temperature curves are shown as stage 5 in Figure 38. For target lines 1-3, typical behavior of gap increases with temperature deceases and then a final gap decrease with a temperature increase. For target lines 1 and 2, this final stage follows along the same slope. For target line 1, this slope is the same as the slope for stages 1 and 3. For target line 2, this final stage has the same slope as stage 3 only. For target line 3 the slope of this final stage changes, initially following the slope of stage 3 and then nearly the slope of stage 1. Target line 4 also returns to the decreasing gap and increasing temperature behavior that is expected in last portion of this stage. In addition, this fnal slope is very similar to the slope of stages 1 and 3.

The somewhat unexpected behavior of the gap compared to the temperature in stage 4 and the changing slopes are likely due to the complex behavior exhibited at the wingwall/diaphragm interface caused by the thermal changes. The movement of the bridge's diaphragm at the interface is likely a combination of longitudinal sliding, movement in the direction of the skew into the wingwall, and rotation. This complex movement cannot be fully measured with the instrumentation installed only on the front face the wingwall/diaphragm interface. The very strange behavior of target line 4 at stage 4 is likely the result of an improper field record.

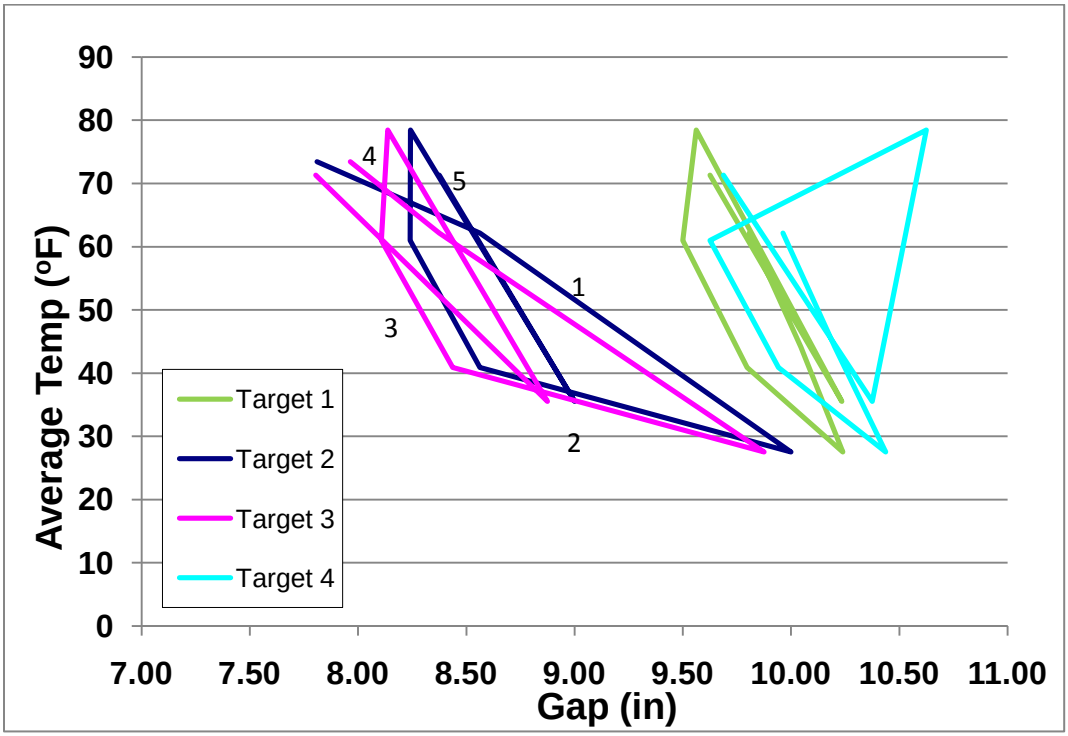

Figure 38: Interfacce Gap vs Average Temperature (DEF-24-0981)

3.3.2 MUS -16-0261

The measured parameters for the MUS-16-0261 bridges are summarized in this section. The measurements include the wingwall/diaphragm interface joint gap, internal temperatures of the wingwall and wall abutments, and the rotation of wall abutments. The movement of the east and west bound bridges was monitored by measuring the gap of the wingwall/diaphragm interface joint in conjunction with measuring the internal temperatures of the wingwalls and wall abutments. The measured wingwall/diaphragm interface joint gap for the east bound bridge is presented in Tables 3 and 4, and that of the west bound bridge is presented in Tables 5 and 6. This data includes the internal temperatures of the south (east bound) and north (west bound) sides of the wall abutment, the wingwall, and an average of the two internal temperatures. In

addition, the lengths of the target gaps are presented in the tables as well. Recall the south wingwall/diaphragm interface (east bound) had two target lines. Target line 1 had targets spaced at approximately 10 in. and target line 2 had targets spaced at approximately 8 in.

Due to problems with instrumentation, temperature data could not be acquired on 7/11/2008. Therefore the temperature of the south end of the east bound wall abutment was taken from nearest the National Oceanic and Atmospheric Administration (NOAA) available data. The temperature for the wingwall of the east bound bridge was then determined by adding or subtracting the average difference between the wingwall and abutment temperatures for all the remaining data points of the east bound bridge. The temperature for the abutment wall of the west bound bridge was then determined by taking the difference in the initial reading of the abutment walls for the east and west bound bridges and subtracting it from the NOAA temperature. The wingwall temperature for the west bound bridge as determined by adding or subtracting the average difference between the wingwall and abutment temperatures for all the remaining data points of the west bound bridge.

Tables 4 and 6 present the difference in the subsequent readings taken relative to the first reading taken after completion of the installation of the targets. The difference in reading was calculated as the subsequent readings minus the initial reading. Thus negative values of ΔT represent decrease in temperatures relative to the first reading, and negative values of the joint movements depict a closing of the joint gaps and an expansion of the bridge superstructure. In addition, positive values of ΔT represent an increase in temperatures relative to the first reading, and positive values of the joint

movements depict an opening of the joint gaps and a contraction of the bridge. Table 6 also shows the change in temperature relative to the installation of the digimatic targets temperature in parenthesis for 9/18/2008 and 11/26/2008.

Table 3: Internal Temperatures and Joint Gap (East Bound MUS-16-0261)

Date	T (Abutment) (^oF)	T (Wingwall) (^oF)	T(Average) (^oF)	Joint Gap 1 (in)	Joint Gap 2 (in)
10/18/2007	68.18	67.28	67.73	9.8241	7.9945
11/14/2007	72.68	68.36	70.52	9.8133	7.9811
2/28/2008	31.46	32.54	32.00	10.0495	8.2125
4/25/2008	63.86	62.42	63.14	9.7996	7.9817
7/11/2008	79.20*	78.81	79.01	9.7257	7.8673
9/18/2008	76.64	79.16	77.90	9.7747	7.9514
11/26/2008	40.1	40.82	40.46	9.9619	8.1368

* Air temperature from NOAA

Table 4: Change in Internal Temperatures and Joint Displacements (East Bound MUS-16-0261)

Date	ΔT (Abutment) (^oF)	ΔT (Wingwall) (^oF)	ΔT(Average) (^oF)	Joint Disp.1 (in.)	Joint Disp.2 (in.)
11/14/2007	4.50	1.08	2.79	-0.0108	-0.0134
2/28/2008	-36.72	-34.74	-35.73	0.2254	0.218
4/25/2008	-4.32	-4.86	-4.59	-0.0245	-0.0128
7/11/2008	11.02	11.53	11.28	-0.0984	-0.1272
9/18/2008	8.46	11.88	10.17	-0.0494	-0.0431
11/26/2008	-28.08	-26.46	-27.27	0.1378	0.1423

Table 5: Internal Temperatures and Joint Gap (West Bound MUS-16-0261)

Date	T (Abutment) (^oF)	T (Wingwall) (^oF)	T(Average) (^oF)	Joint Gap (in.)
10/18/2007	65.12	65.48	65.3	-
11/14/2007	52.88	51.80	52.34	-

2/28/2008	25.16	25.88	25.52	-
4/25/2008	66.38	66.02	66.2	-
7/11/2008	76.14	76.08	76.11	8.0028
9/18/2008	65.48	65.30	65.39	8.1006
11/26/2008	37.58	37.76	37.67	8.2252

Table 6: Change in Internal Temperatures and Gap Displacements (West Bound MUS-16-0261)

Date	ΔT (Abutment) (^{o}F)	ΔT (Wingwall) (^{o}F)	ΔT(Average) (^{o}F)	Joint Disp. (in.)
11/14/2007	-12.24	-13.68	-12.96	-
2/28/2008	-39.96	-39.6	-39.78	-
4/25/2008	1.26	0.54	0.90	-
7/11/2008	11.02	10.60	10.81	-
9/18/2008	-10.66	-10.78	-10.72	0.0978
11/26/2008	-38.56	-38.32	-38.44	0.2224

As shown in Table 4, it can be seen that the largest east bound joint gap closing measured during the course of the research occurred at target line 2 and was 0.1272 in. This corresponds to the largest temperature increase recorded, and the bridge was also expected to expand the most during that period. The largest east bound joint displacement opening measured occurred at joint gap 1 and was 0.225 in. This value corresponds to the largest temperature decrease recorded during the period of data acquisition. During this period, the bridge was expected to contract the most.

Though the installation of targets on the west bound bridge came later during the research, some data was collected with regards to opening and closing of the joint. As can be seen in Table 6, the west bound joint gap opening measured was 0.2224 in. By comparing the measurements of the east bound bridge with that of the west bound bridge,

it is apparent that the wingwall of the west bound bridge experienced more changes in internal temperatures than that of the east bound bridge.

The temperatures from the abutment and the wingwall varied by less than a few degrees for the east bound and west bound bridges with the west bound bridge showing less variation. The temperatures were typically higher for the east bound bridge compared to the west bound bridge. This was likely caused by position of the bridges relative to the sun. The east bound bridge wingwall and abutment are often directly exposed to sunshine while the west bound bridge being shaded by the deck. The only exception was 4/25/2008 where the north was actually warmer than the south. In addition, the north side of the wall abutment for the west bound bridge experienced larger changes in the internal temperatures than the south side of the wall abutment for the east bound bridge. This is partly because the bridge superstructure provided more shade to the reference points of the east bound bridge. Thus it would be expected that the wingwall/diaphragm opening and closing of the west bound bridge would be greater than that of the east bound bridge.

Plots of the wingwall/diaphragm interface joint gaps versus the average internal temperatures of the wingwall and wall abutment were created in order to determine if a correlation that existed between the aforementioned parameters. The plots were only created for the south (east bound) bridge because of limited data for the north (west bound) bridge. The average temperature was used since there were only minor differences in the temperatures between the wingwall and abutment. Target line 1 was used since there were limited differences between target lines 1 and 2. Additional plots can be found in Shehu (2009). Figure 39 is a plot of the actual wingwall/diaphragm interface gap verses the average temperature. As expected the

gap length increases as the temperature deceases. Figure 40 shows the plot of the change in the wingwall/diaphragm interface gap verses the average temperature change. Shehu (2009) fit linear regression lines to Figures 39 and 40 as well as other figures for the data. The linear regression lines had correlation coefficients in excess of 0.9.

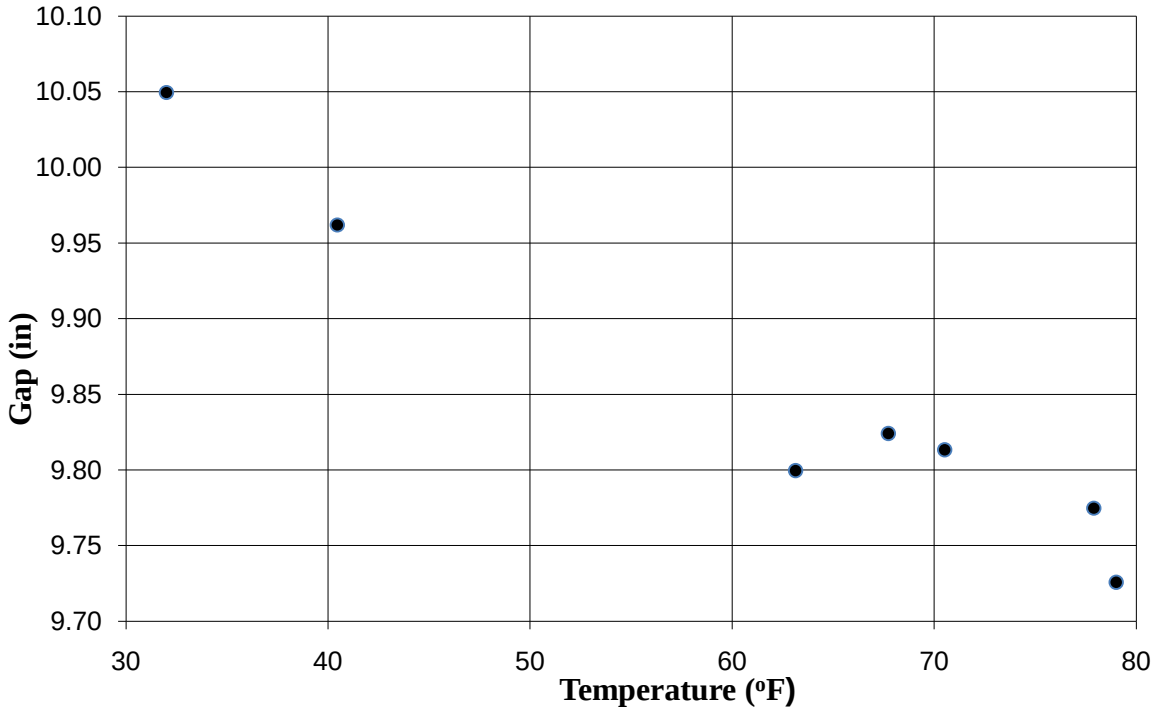

Figure 39: Joint 1 Gap versus Average Temperature (East Bound MUS-16-0261)

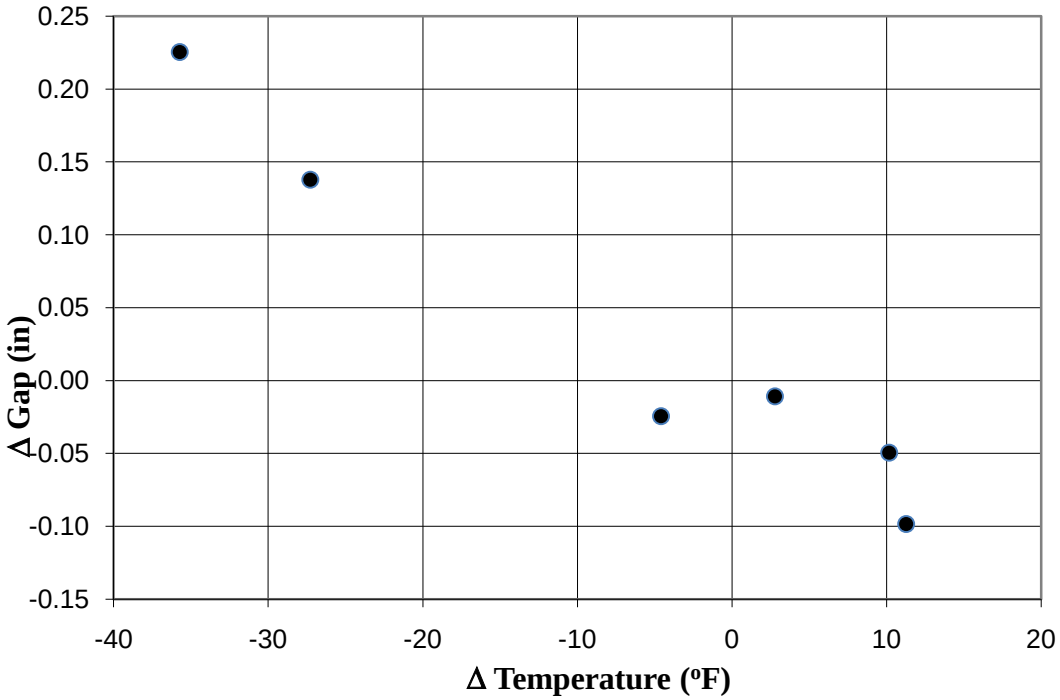

Figure 40: Joint 1 Displacement versus Average Temperature (East Bound MUS-16-0261)

The tilting of the abutment walls and wingwalls for the east and west bound bridges were also measured for the bridge MUS 16-0261. The initial tilt-meter measurements were taken on October 18th 2007. This was the date the tilting reference stainless steel studs were installed. Tables 6 and 7 provide the tilt measurements for the east and west bound bridges, respectively. The measurements were taken at two locations on each abutment wall denoted north and south and one location on each wingwall (see Figures 27 and 28). As previously stated, the tilt angle measured using the tilt-meter is the angle with respected to the vertical. Positive measurements indicate that the wall is leaning away from the backfill, while negative measurements indicate that the wall is leaning toward the backfill. As can be seen in Tables 7 and 8, all readings are negative implying all the walls lean toward the backfill slightly. In addition, the measured tilt

angles ranged from 0.191^{o} to 0.662^{o} for the abutment and 0.597^{o} to 0.976^{o} for the wingwall of the east bound bridge. The range of tilt for the west bound bridge is 0.112^{o} to 0.503^{o} for the abutment and 0.430^{o} to 1.142^{o} for the wingwall.

Table 7: Abutment and Wingwall Tilt (East Bound MUS-16-0261)

Date	Abutment (North) (deg)	Abutment (South) (deg)	Wingwall (deg)
10/18/2007	-0.261	-0.639	-0.629
11/14/2007	-0.264	-0.650	-0.597
2/28/2008	-0.233	-0.637	-0.604
4/25/2008	-0.271	-0.642	-0.976
7/11/2008	-0.223	-0.662	-0.925
9/18/2008	-0.191	-0.657	-0.646

Table 8: West Abutment and Wingwall Tilt (West Bound MUS-16-0261)

Date	Abutment (North) (deg)	Abutment (South) (deg)	Wingwall (deg)
10/18/2007	-0.112	-0.342	-0.723
11/14/2007	-0.498	-0.437	-0.430
2/28/2008	-0.127	-0.375	-0.496
4/25/2008	-0.503	-0.427	-0.672
7/11/2008	-0.427	-0.427	-0.688
9/18/2008	-0.119	-0.425	-1.142

Tables 9 and 10 present the change in tilt measurements along with the change in average temperatures for the east and west bound bridges, respectively. It was expected that when the bridge undergoes thermal expansion, the abutments would move towards the backfill while the wingwall moves away from the backfill. However by referring to Table 9, it can be seen that this is not always the case. For the first date of Table 9, the temperature rose slightly and the abutment moved into the backfill as the wingwall moved away from the backfill. On 2/28/2008,

the data shows a large drop in temperature, with the abutment moving away from the backfill and the wingwall leaning away from the backfill less than on 11/24/2007 but not less than it initially did. The next sampling date, 4/25/2008, had a higher temperature than the previous date but still less than the initial temperature. The abutment and wingwall tilt toward the backfill more than its initial reading. The data for 7/11/2008 had the highest temperature and showed the south abutment reading to tilt toward the backfill, as would be expected. However, the data acquired from the north side of this abutment shows the abutment leaning its most significant amount away from the backfill. The wingwall also tilts toward the backfill more than initially. Similar behavior was exhibited on 9/18/2008.

The results for the west bound bridge, shown in Table 10, do not behave as expected either. The first two dates of data show temperature decreases with the abutment leaning more into the backfill and the wingwall leaning more away from the backfill. This is just the opposite as would be expected. The last two dates of the data show expected behavior and consistant behavior of the wingwall relative to the abutment wall.

Thus it can be surmised that the movement of the wingwalls and abutments towards and away from the backfill is very complex. This complex behavior is likely due to the nonlinear movement of the abutments and wingwalls relative to the temperature. The temperatures were also taken at a point in time and the history of the temperature several days prior to the measurements may also influence behavior. The upper portion of the bridge (deck and superstructure) may vary significantly compared to the locations used for temperature measurements. The bridge may also exhibit different behavior from one end to the other.

Table 9: Abutment and Wingwall Tilt Changes (East Bound MUS-16-0261)

Date	ΔT(Average) (^{o}F)	Abutment (North) (deg)	Abutment (South) (deg)	Wingwall (deg)
11/14/2007	2.79	-0.003	-0.011	0.032
2/28/2008	-35.73	0.027	0.001	0.024
4/25/2008	-4.59	-0.010	-0.003	-0.347
7/11/2008	11.28	0.037	-0.023	-0.297
9/18/2008	10.17	0.070	-0.019	-0.017

Table 10: Abutment and Wingwall Tilt Changes (West Bound MUS-16-0261)

Date	ΔT(Average) (^{o}F)	Abutment (North) (deg)	Abutment (South) (deg)	Wingwall (deg)
11/14/2007	-12.96	-0.387	-0.095	0.294
2/28/2008	-39.78	-0.016	-0.034	0.228
4/25/2008	0.90	-0.391	-0.085	0.052
7/11/2008	10.81	-0.315	-0.085	0.036
9/18/2008	-10.72	0.380	0.011	-0.712

CHAPTER 4: ANALYTICAL ASSESMENT

In performing the analytical aspect of this research, a computer software program was used to carry out a finite element (FE) analysis. SAP 2000, a structural engineering software that is capable of performing both FE analysis and design, was utilized to analyze the response of the bridge deck and the wingwall. Due to the fact the MUS-16-0261 bridge has already shown signs of distress and has also experienced movement before instrumentation, the initial conditions were unknown and thus could not be fully accounted for in the analysis. In addition, the actual behavior is affected by numerous parameters and lead to a complex system that is nearly impossible to truly model. For this reason, it is very difficult to make a direct comparison between the computer analysis and the field analysis. Since several assumptions were made to account for the initial conditions of the MUS-16-0261 bridge as well as the numerous parameters that effect the behavior of these bridges, the computer analysis is considered a parametric study and was performed for the purpose of gaining more insight on the magnitude of the forces that could potentially be generated and transferred to the wingwalls and to better understand the distribution of the stresses on the walls.

4.1 System Analysis

Finite element analyses were performed on bridge systems using multiple bridge spans with different skew angles and varying backfill soil stiffness values. Span lengths of 139 ft., 200 ft., 400 ft. and 600 ft. each with skew angles 15^o, 30^o, 45^o and 60^o were all modeled in the computer software with the different backfill soil stiffness values. Though according to the 2007 Ohio Bridge Design Manual, the maximum span length allowable for a semi-integral bridge with a combination of skew angle from 0^o-50^o is 400 ft. (see Figure 4), a 600 ft. span was analyzed in order to investigate this specified limitation. Likewise, the maximum allowable skew angle as presented in the 2007 Ohio Bridge Design Manual is 50^o. The justification for this limitation was investigated as well with the analyses of 60^o skews. The 139 ft. long bridge deck modeled the field monitored MUS-16-0261 bridge. It should be noted that the length of 139 ft. is the span

length from center to center of the bearing support, and this is true of all the lengths of the models analyzed.

Several assumptions were made in order to model the deck of the bridge into the FE software. The entire length of the bridge was modeled for analysis by dividing the deck into small rhombus shaped thin-shell elements due to the skew (see Figure). The deck shells were created using a 4.5ksi normal weight (150 pcf) concrete. The value of modulus of elasticity (E) for the concrete was 3.82 x 10^3 ksi as determine using the compressive strength of the concrete and equation 6 below.

$$E = 57{,}000\sqrt{f'_c} \qquad (6)$$

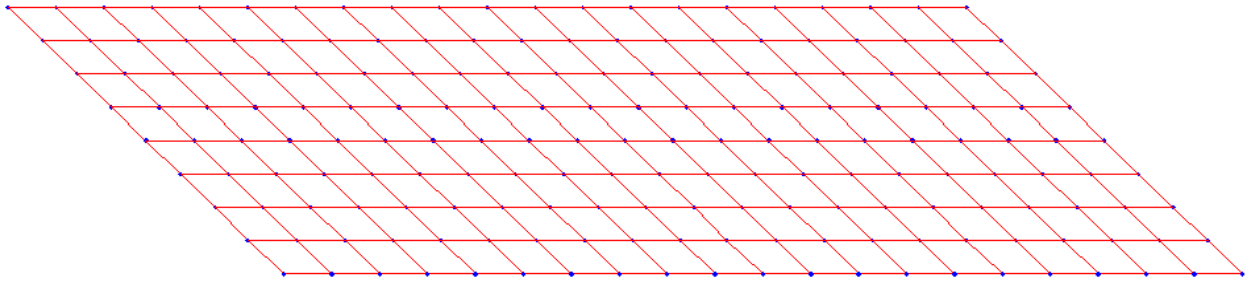

Figure 41: Deck Divided into Rhombus Shell Elements

As explained by MacGregor and Wight (2005), the range of values for poison's ratio (ν) of concrete is usually from 0.11 to 0.21 and the coefficient of thermal expansion (α) of normal weight concrete is from 5 to 7 x 10^{-6} strain/^{o}F. MacGregor and Wight (2005) also added that "an all around value of 5.5 x 10^{-6} strain/^{o}F may be used". Thus, default values of 0.2 and 5.5 x 10^{-6} strain/^{0}F were used in the analyses for poison's ratio and coefficient of thermal expansion, respectively.

The girder sections for the MUS-16-0261 bridge were grade 50 ASTM A572 welded steel plate girders, which were created in the program based on the dimensions of the plates given in the drawings. This was done because the sizes of the girders used in the project were not available in the software library. According to Metal Suppliers Online, a mean value of thermal coefficient is 6.7 x 10^{-6} strain/^{o}F and an elastic modulus of 30 x 10^6 psi were used for the material. In addition, a yield strength value of 50 ksi was used since the material is grade 50.

All girder sections were divided into element lengths of the same size as the rhombus thin-shell elements.

The resistance to motion in the X and Y directions was modeled as linear springs (see Figure 42). This was done to model the restraining effects on the diaphragms.

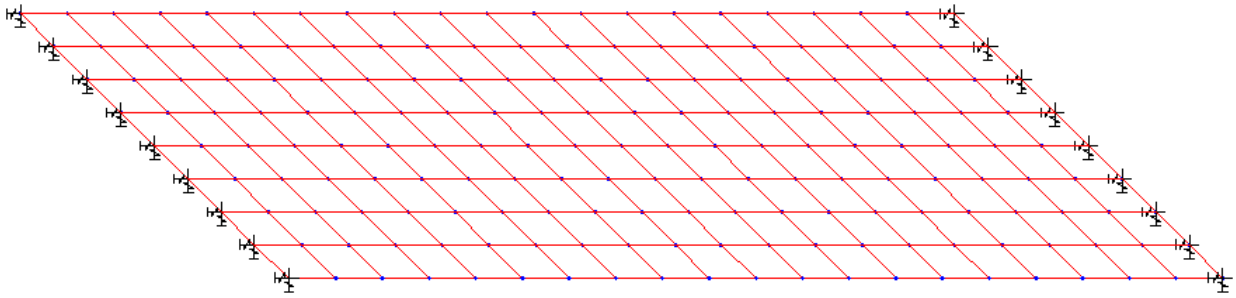

Figure 42: Resistance Modeled with Linear Springs

Though the stiffness value for the granular backfill material was not presented in the literature, stiffness values for sands were assumed (Bowles, 2005). Stiffness values of 35.37 lb/in^3, 100.57 lb/in^3, and 165.78 lb/in^3 were assumed based on similar research conducted by Bettinger (2001). The wide range of stiffness values investigated could also be thought of as an equivalent stiffness to take into account the resistance resulting from other sources other than the compression of the backfill such as the shearing resistance of the bearing pads, the frictional resistance of the backfill on the superstructure, and the effects of the approach slab. The equivalent stiffness values were converted into spring stiffness/support (kip/in) in the X and Y directions. The calculations carried out in converting the stiffness values are presented below. The contact area (A_C) between the diaphragm and backfill was determined by Equation (7). This equation used the dimensions of the MUS-16-0261 bridge and would vary from bridge to bridge.

$$A_C = \left(\frac{W_D \times H_D}{\cos(\theta)} \right) = \left(\frac{42\ ft \times 6.33\ ft}{\cos(\theta)} \right) \qquad (7)$$

where:

θ = skew angle (degrees)

W_D = width of diaphragm

H_D = height of diaphragm

The Stiffness/Support was determined from Equation (8).

$$\text{Stiffness/Support} = \left(\frac{SS \times A_C}{n \cos(\theta)} \right) \quad (8)$$

where:

SS = equivalent stiffness taken as 35.37 lb/in^3, 100.57 lb/in^3, or 165.78 lb/in^3

n = the number of support nodes at the end of the bridge model

A total of nine springs were evenly spaced along the width of diaphragms for all the models with the exception of 139 ft and 200 ft with a skew angle of 60^o. These two models had a total of 17 springs evenly spaced along the width of the abutment. Thus, n = 9 or 17 where appropriate. The spring stiffness were then broken down into their respective X and Y components using Equations (9) and (10).

$$X_{comp} = (\text{Stiffness/Support}) \cos\theta \quad (9)$$

$$Y_{comp} = (\text{Stiffness/Support}) \sin\theta \quad (10)$$

The stiffness values used in the modeling are summarized in Table 11. It should be noted that the behavior of the resistance is more complex than the assumptions made in order to create the models for the analyses. However, for the purposes of this research, the simplifying assumptions made to create the models were adequate to assist in comparing the analyses results with the field data.

Table 11: Equivalent Stiffness to Spring Stiffness Conversion

# of Springs	θ (^{o})	Equiv. Stiffness (lb/in^3)	A_c (ft^2)	Stiffness /Support (lb/in^3)	X_{comp} (lb/in^3)	Y_{comp} (lb/in^3)
9	15	35.37	275.24	161.26	155.76	41.74
9	15	100.57	275.24	458.52	442.89	118.67
9	15	165.78	275.24	755.82	730.06	195.62
9	30	35.37	306.99	200.61	173.73	100.30
9	30	100.57	306.99	570.40	493.98	285.20
9	30	165.78	306.99	940.25	814.28	470.13
9	45	35.37	375.98	300.91	212.78	212.78
9	45	100.57	375.98	855.60	605.00	605.00
9	45	165.78	375.98	1,410.38	997.29	997.29
9	60	35.37	531.72	601.82	300.91	521.19
9	60	100.57	531.72	1,711.20	855.60	1.481.94
9	60	165.78	531.72	2,820.75	1,410.38	2,442.84
17	60	35.37	531.72	318.61	159.31	275.93

17	60	100.57	531.72	905.93	452.97	784.56
17	60	165.78	531.72	1,493.34	746.67	1,293.27

The 2 in. thick preformed expansion joint filler (PEJF) used between the wingwall/abutment interface was also modeled as a linear spring at the acute corners of the bridge model. To determine the stiffness of that spring, compression testing was performed by Ohio University on the PEJF. The results of the testing are presented in Table 12. The test required that the PEJF material be able to support a 250 psi compressive stress at 50% compression deformation of the material. The PEJF test sample size was 4 in. x 4 in. and thus had an area of 16 in^2. The differences in the two tests shown in Table 12 was that the Test 1 samples were tested at laboratory temperature and the Test 2 samples were tested at 95 ^oF. This also required the use of two different compression machines. As can be seen in Table 12, the temperature did not affect the behavior of the PEJF.

The results of Table 12 were determined using abutment/wingwall interface dimensions of the MUS-16-0261 bridges. The wingwall/diaphragm interface area for the east and west bound MUS-16-0261 bridges were 2,734.56 $in.^2$ and 3,283.2 $in.^2$, respectively. As can be seen from Table 12, the average magnitude of force required to compress the PEJF by 1 in. for the east and west bound MUS-16-0261 bridges were 709 kips and 851 kips, respectively. The stress associated with these forces as determined in the testing was 259 psi. Since this stress exceeds the maximum required stress of 250psi in the PEJF, the forces at each wingwall required to compress the PEJF by 1 in. were back calculated using a compressive stress of 250 psi at the abutment/wingwall interface. Spring stiffness values at the acute corners of the east and west bound MUS-16-0261 bridges were thus determined to be 685 kip/in and 820 kip/in, respectively. These values of 685 kip/in and 820 kip/in were used instead of 709 kip/in and 851 kip/in because they represent the maximum stress value of 250 psi in the PEJF. In addition 685 kip/in and 820kip/in are conservative values since based on the test, the material can withstand 259 psi of stress, but the value was reduced to 250 psi.

Table 12: PEJF Test Results

Test 1 Results					
Initial Thickness (in)	Thickness After 10 min. Recovery Period (in)	Load Required to Compress to 50% of Thickness (lbs)	PEJF Stresses (psi)	Forces at East Wingwall (kips)	Forces at West Wingwall (kips)
1.022	0.854	3925	245	671	805
1.034	0.868	3985	249	681	818
1.008	0.846	4417	276	755	907
1.032	0.864	3996	250	683	820
2.078	1.724	4407	275	753	904
2.054	1.678	4528	283	774	929
Average =		**4146**	**259**	**709**	**851**
Test 2 Results					
1.015	0.805	4552	285	778	934
1.002	0.812	4405	275	753	904
1.031	0.867	3492	218	597	717
Average =		**4150**	**259**	**709**	**852**

The supports at the approach ends of the decks were modeled as rollers to allow for thermal expansion and contraction. According section 3.12.2 of the Ohio Bridge Design Manual, a base construction temperature of 60^{o}F shall be assumed for design purposes. A 60^{o}F temperature change was imparted on the deck and girders of the bridge models assuming bridge temperatures would not exceed 120^{o}F.

The results of the FEM analyses carried out on the bridge models are presented in Tables 13 and 14 for the east and west wingwalls, respectively. As shown by the data in the Tables, the stress in the wingwall only exceeds 250 psi at long spans with high skews for the assumed soil stiffness values.

Table 13: Forces and Stresses in East Wingwall

		Equivalent Stiffness (lb/in^3)			Equivalent Stiffness (lb/in^3)		
		35.37	100.57	165.75	35.37	100.57	165.75
Skew	Length	East Wingwall Forces			East Wingwall Stresses		

	(ft)	(kips)			(psi)		
15°	139	58	96	125	21	35	46
	200	63	105	138	23	38	50
	400	77	134	180	28	49	66
	600	92	164	222	34	60	81
30°	139	99	159	205	36	58	75
	200	117	188	243	43	69	89
	400	173	275	348	63	101	127
	600	226	348	429	83	127	157
45°	139	190	253	312	69	93	114
	200	216	308	374	79	113	137
	400	338	454	525	124	166	192
	600	443	351	623	162	205	228
60°	139	214	251	280	78	92	103
	200	263	300	413	96	110	151
	400	478	584	645	175	214	236
	600	616	693	734	225	254	268

Table 14: Forces and Stresses in West Wingwall

		Equivalent Stiffness (lb/in^3)			Equivalent Stiffness (lb/in^3)		
		35.37	100.57	165.75	35.37	100.57	165.75
Skew	Length (ft)	West Wingwall Forces (kips)			West Wingwall Stresses (psi)		
15°	139	63	103	132	19	31	40
	200	63	106	139	19	32	42
	400	83	142	188	25	43	57
	600	98	173	230	30	53	70
30°	139	107	170	215	33	52	66
	200	126	200	255	38	61	78
	400	186	291	363	57	89	110
	600	242	368	446	74	112	136
45°	139	176	270	328	53	82	100
	200	234	327	392	71	100	119
	400	365	482	550	111	147	167

	600	478	583	651	146	178	198
60°	139	236	272	300	72	83	91
	200	289	326	427	88	99	130
	400	527	618	672	160	188	205
	600	666	732	764	203	223	233

Plots were generated as shown in

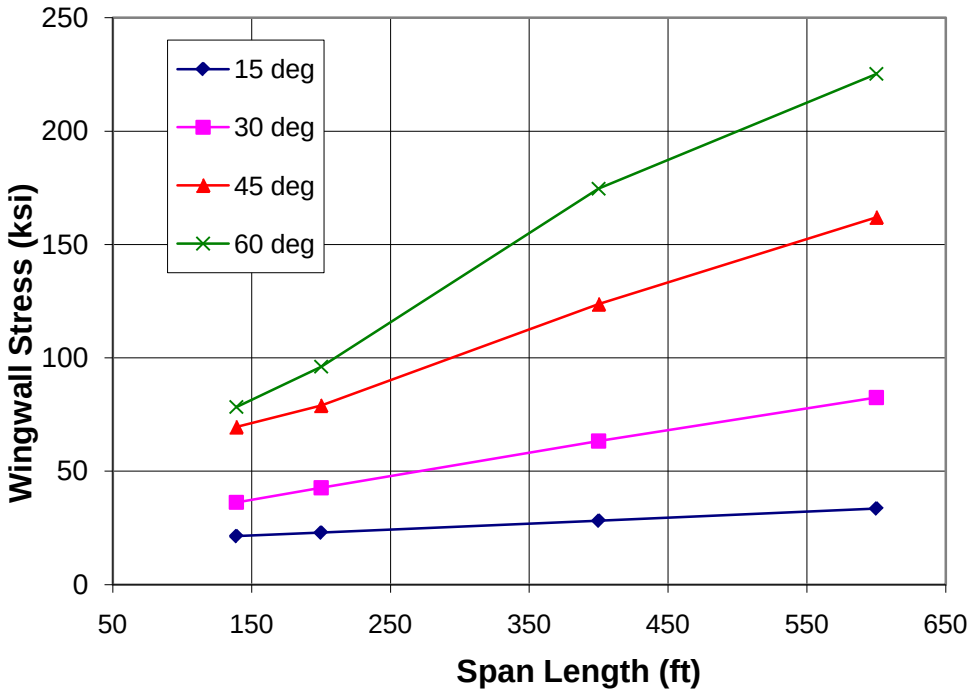

Figure Figures 43 - 45 to investigate the effect of varying the length of superstructure, the skew angle, and the equivalent stiffness on the wingwall stresses for different skews. The difference in Figures 43 - 45 is the assumed equivalent stiffness.

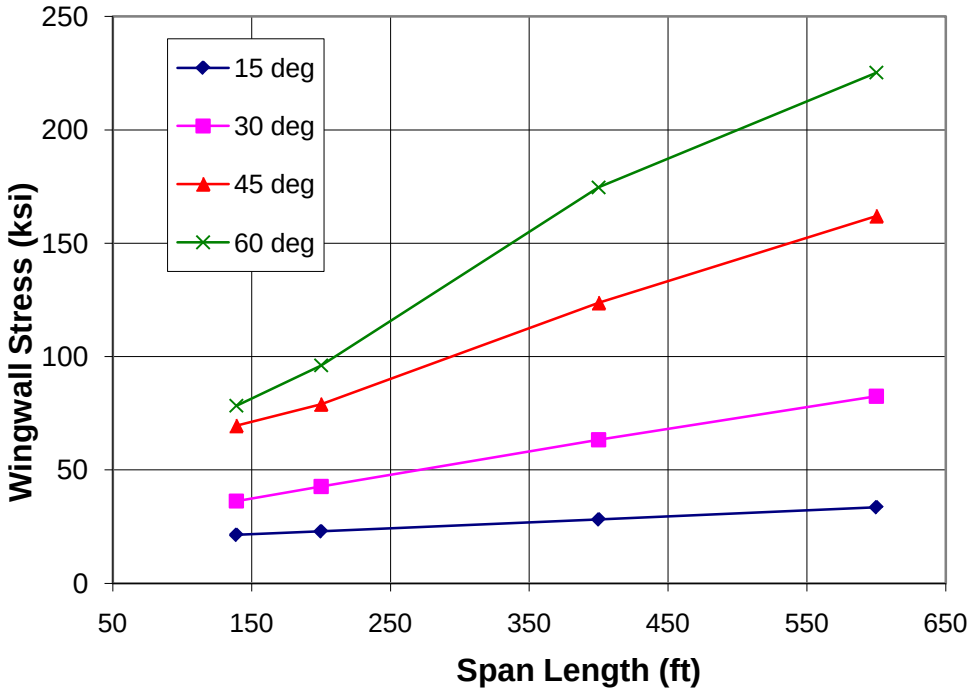

Figure 43: Span Length on Stresses for Different Skews (k_{Eq} = 35.7lb/in^3)

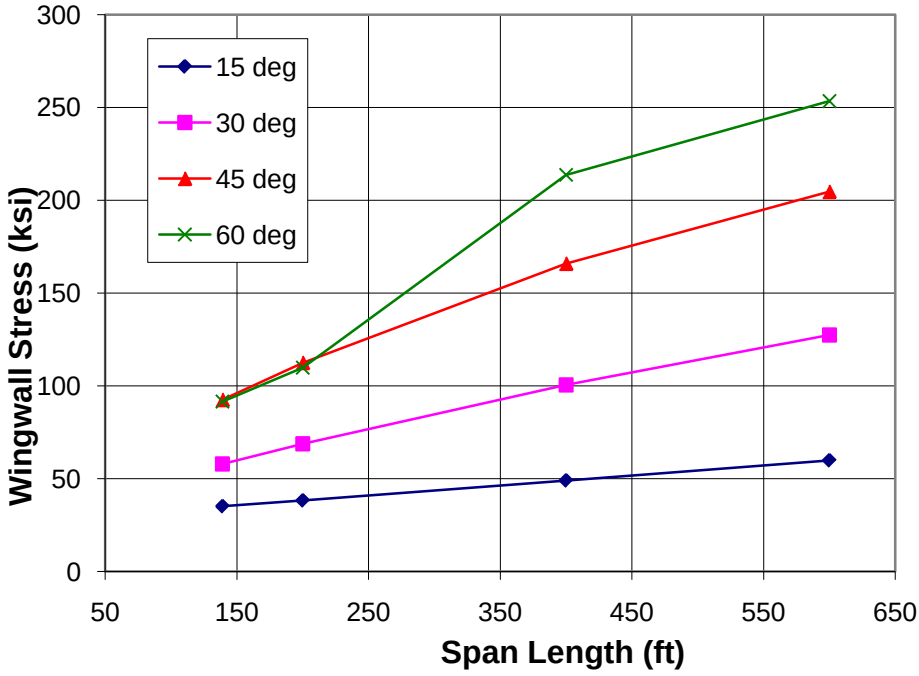

Figure 44: Span Length vs Stresses for Different Skews (k_{Eq} = 100.57lb/in^3)

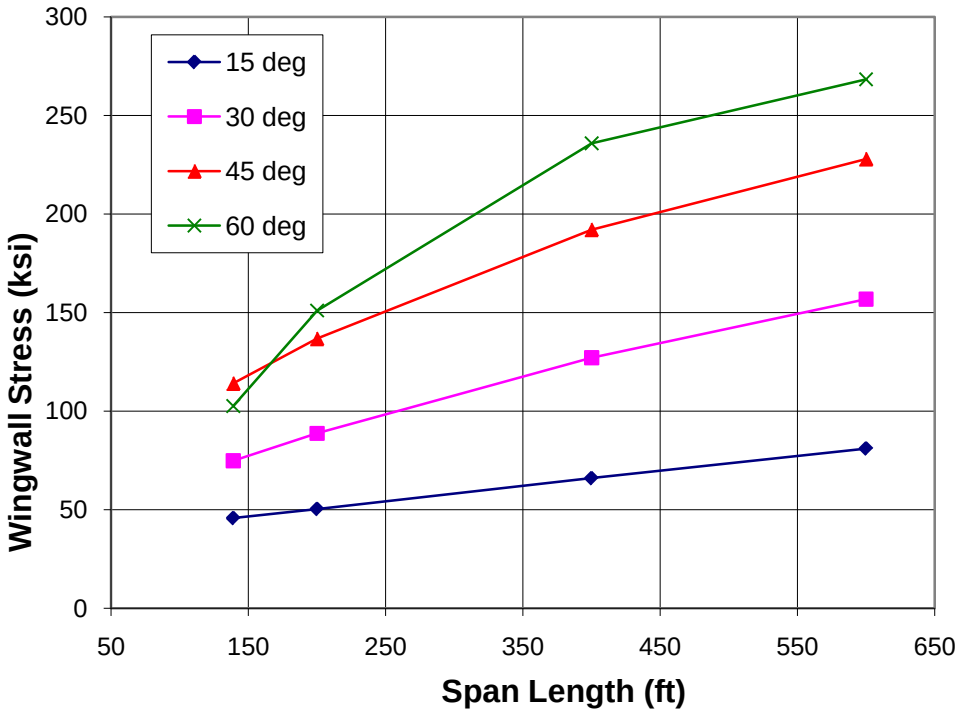

Figure 45: Span Length vs Stresses for Different Skews (k_{Eq} = 165.75 lb/in^3)

From Figures 43-45, the higher equivalent stiffness produces a higher stress but the difference in magnitudes is not that significant for the range of values investigated. The majority of models investigated showed a range within 50 psi for the skews and spans modeled.

The longer spans produce larger stresses and the effect becomes more pronounced for the higher skews. At the skew of 15^o, stresses increased less than 50 psi for the range of spans investigated. However at a 45^o skew, the stresses increased over 100 psi for the span range analyzed.

The skew has affects the stresses significantly when the spans are long. Even at spans of 139 to 200 feet, the stresses increase b 80 psi from 15^o to 45^o. At the longer 400 and 600 foot spans the stresses increase by well over 100 psi for the 15^o to 45^o skews.

Table 15 provides the movement at the abutment wall-wingwall interface for the model with the 45^o skew and the span of 139 ft. The values of the analytical study can be compared to the results of the field study shown in Tables 3 and 5. The largest joint displacements measured in the field were approximately 0.22 in. with a 37 ^{o}F temperature

change. The analytical results show similar magnitude wall joint movements for the models with the 60°F temperature change leading to some justification of the assumed equivalent stiffness values assumed. The lower equivalent stiffness of 35.37 lb/in^3 show slightly higher movements and may be more representative of the actual field instrumented bridge, MUS-16-0261. Differences in the joint movements can also be attributed to instrumentation being installed well after the bridge was constructed and experienced numerous daily and seasonal thermal cycles.

Table 25: Analytical Wall Joint Movement (45° skew and Span = 139 ft.)

Equivalent Stiffness (lb/in^3)	East Joint Movement (in)	West Joint Movement (in)
35.37	0.249	0.242
100.57	0.223	0.219
165.75	0.204	0.203

4.2 Wingwall and Wall Abutment Interface

A FE model of the wingwall and wall abutment was created by utilizing SAP 2000 (see Figure 46). The analysis was carried out to investigate the magnitude and stress distribution pattern at the abutment/wingwall interface and on the surface of the wingwall and wall abutment. The wingwall and wall abutment model was broken into 1,728 solid elements and the base support of the walls was assumed fixed. The solid elements were created using a 4.5 ksi normal weight concrete (150pcf) as given in the project drawings. As aforementioned, the value of modulus of elasticity (E) used was 3.82 x 10^3 ksi.

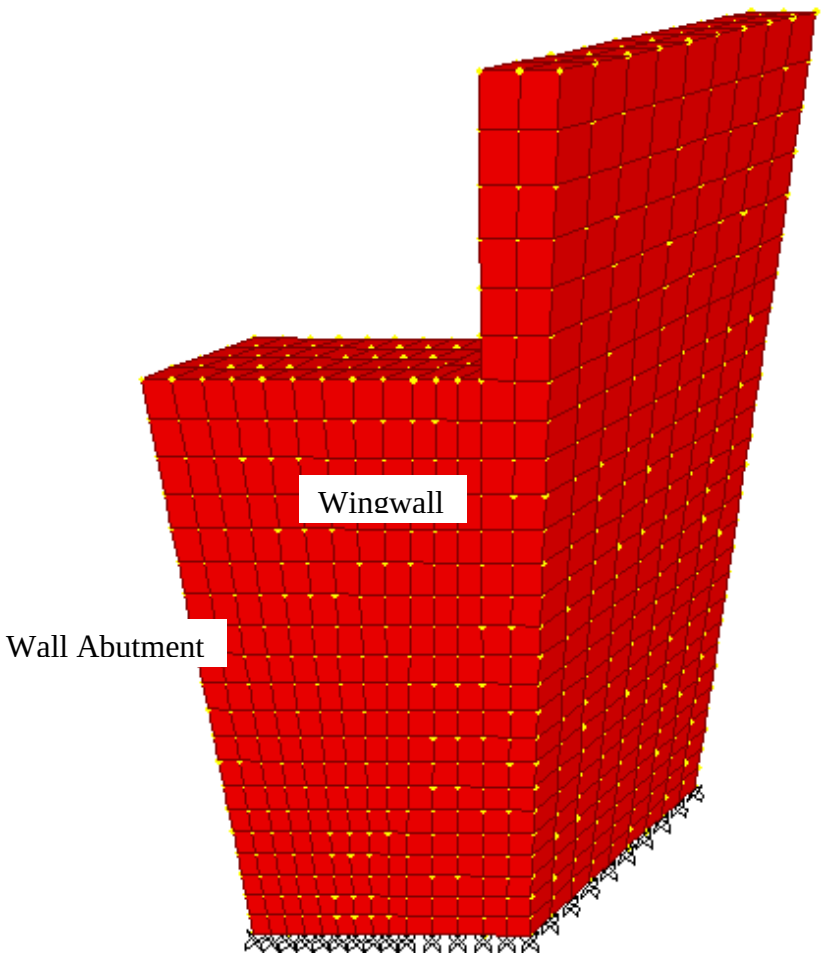

Figure 46: Wingwall and Wall Abutment Model

Only 9 ft. of both the wingwall and wall abutment lengths were modeled. This was done since the primary interest was the interface between the walls and to reduce the model size along with the associated computing time of the analysis. A poison's ratio (ν) and coefficient of thermal expansion (α) values of 0.2 and 5.5 X 10^{-6} strain/^{o}F, respectively (MacGregor and Wight, 2005) were used.

The loads considered during this analyses included the self weight of both the wingwall and wall abutment, the dead weight of the deck and girders supported by each abutment, the lateral earth pressure from the backfill acting on both the wingwall and wall abutment and a 100 psi pressure from the diaphragm acting on the wingwall at the abutment/wingwall interface.

The following equations were used to calculate the lateral earth pressure of the backfill against the wingwall and wall abutment (Budhu, 2008). Rankine's theory of active earth pressure was used. This is because the passive case (wall pushing against soil) is an extreme situation and unlikely to be the mode in this case. Passive case is possible when the deck expands at higher temperatures. Figure47 shows a diagram of the wall and embankment backfill soil.

Equation 11 was used to calculate the active earth pressure coefficient. K_{aR} was determined to be 0.337 using values of $\beta = 0$, $\eta = 2.9^o$ and an assumed value of $\phi' = 30^o$. The value of ϕ' was assumed within the 28^o-33^o typical range of ϕ' for granular soils (Budhu, 2008). The value of ϕ_a needed to evaluate Equation 11 was determined from Equation 12. K_{aR} of 0.337 was found to be close to the typical values determined from similar parameters (Bowles, 1996).

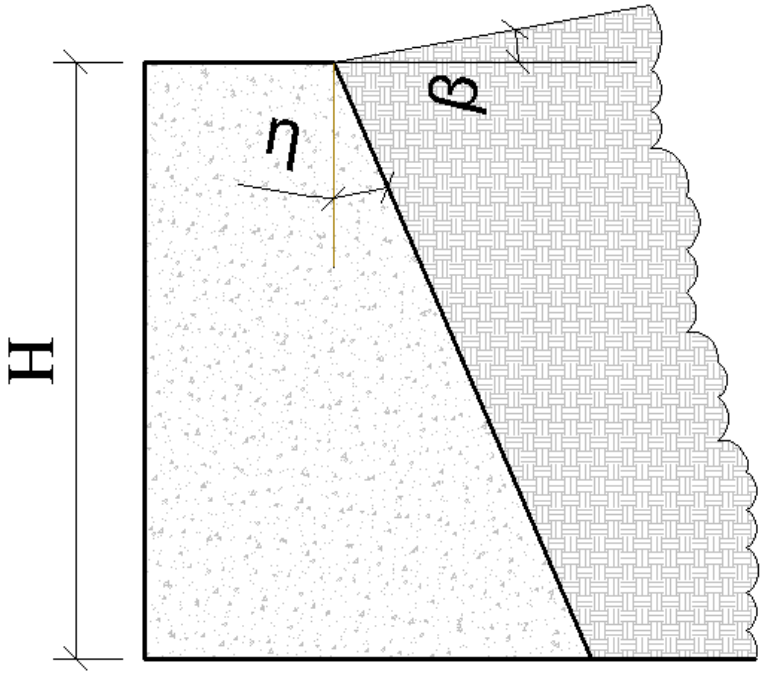

Figure 47: Wall and Backfill

$$K_{aR} = \frac{\cos(\beta - \eta)\sqrt{1 + \sin^2\phi' - 2\sin\phi'\cos\varphi_a}}{\cos^2\eta\left(\cos\beta + \sqrt{\sin^2\phi' - \sin^2\beta}\right)} \qquad (11)$$

where:

K_{aR} = Rankine's Active Earth Pressure Coefficient

ϕ' = Internal Friction Angle

$$\varphi_a = \sin^{-1}\left(\frac{\sin\beta}{\sin\phi'}\right) - \beta + 2\eta \quad (12)$$

The pressure was then determined using Equation 13

(with an assumed value of 120 pcf for the soil unit weight, γ. This assumed value for the unit soil weight was within the 106 pcf – 125 pcf typical range for sands (Bowles, 2005).

$$P_{soil} = K_{aR} \cdot \gamma \cdot h \quad (13)$$

where:

P_{soil} = Soil pressure at a given height

γ = Unit weight of soil

h = height

The soil pressure acting on the face of each solid element was determined by first calculating the pressure at the top and bottom of each solid element, and then taking the average between the two pressures. The difference between the pressure at the top and bottom of each solid element was small. Thus, the elements were considered small enough to assume that the pressure distribution within a solid element was constant throughout the element.

The 100 psi pressure at the diaphragm/wingwall interface was selected based on the majority of field measurements were at or below this value and the analytical assessments of the bridge systems only exceeded 100 psi at large spans and skews. In addition, the analyses of the bridge systems were based on an assumed equivalent stiffness resisting the thermal induced movement as well as a ΔT of 60^{o}F. The PEJF laboratory testing resulted in stresses near 250 psi. However, this was when the compression of the specimen was at one-half its original thickness of 2". Field results did not show compression of the diaphragm/wingwall interface as high as 1".

The model for a portion of the abutment wall and wingwall was analyzed once the necessary assumptions and restraints were imposed and the application of the aforementioned loads was completed. Figure 48 shows the deflected shape of the model at the completion of the analysis.

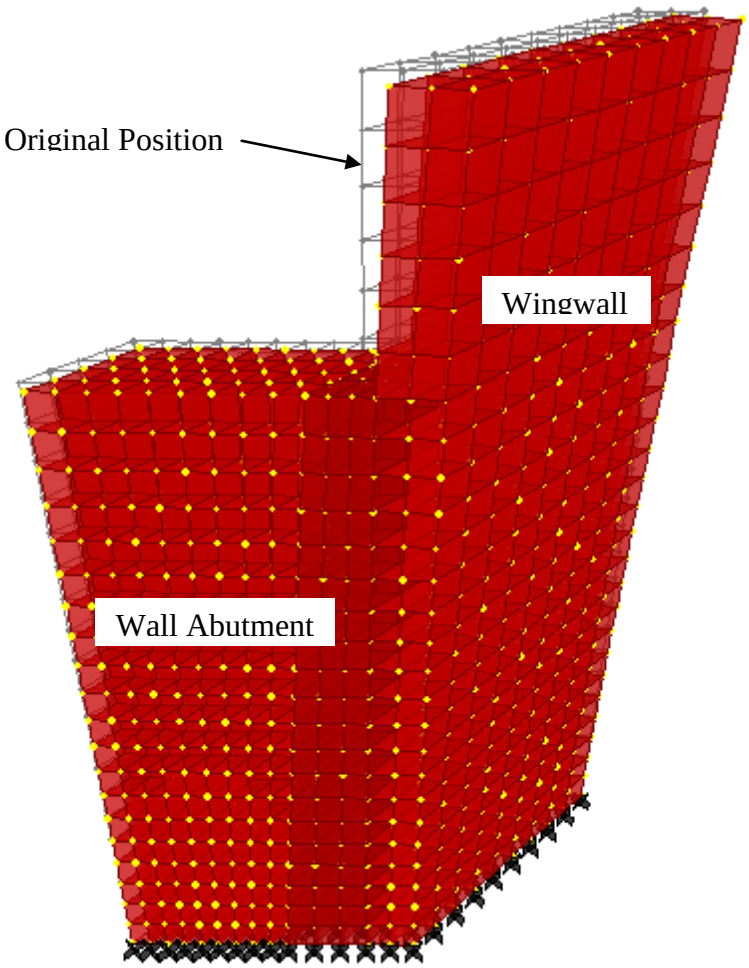

Figure 48: Wall Abutment and Wingwall Deformation

By making reference to the deflected of the structure, it can be seen that the front side of the wingwall is in compression while the back side is in tension. This is due to the direction of the applied lateral earth pressure acting on the back side as well as the 100 psi load from the diaphragm. In addition, it can be seen that the top of the wall abutment

deformed downward slightly due to the applied deck self-weight. Also, the front side of the abutment wall is in compression and backside is in tension due to lateral earth pressure of the backfill acting on the backside. Figure 49 and 50 show the distribution of vertical normal stresses on the front side and the backside of the wall panels, respectively.

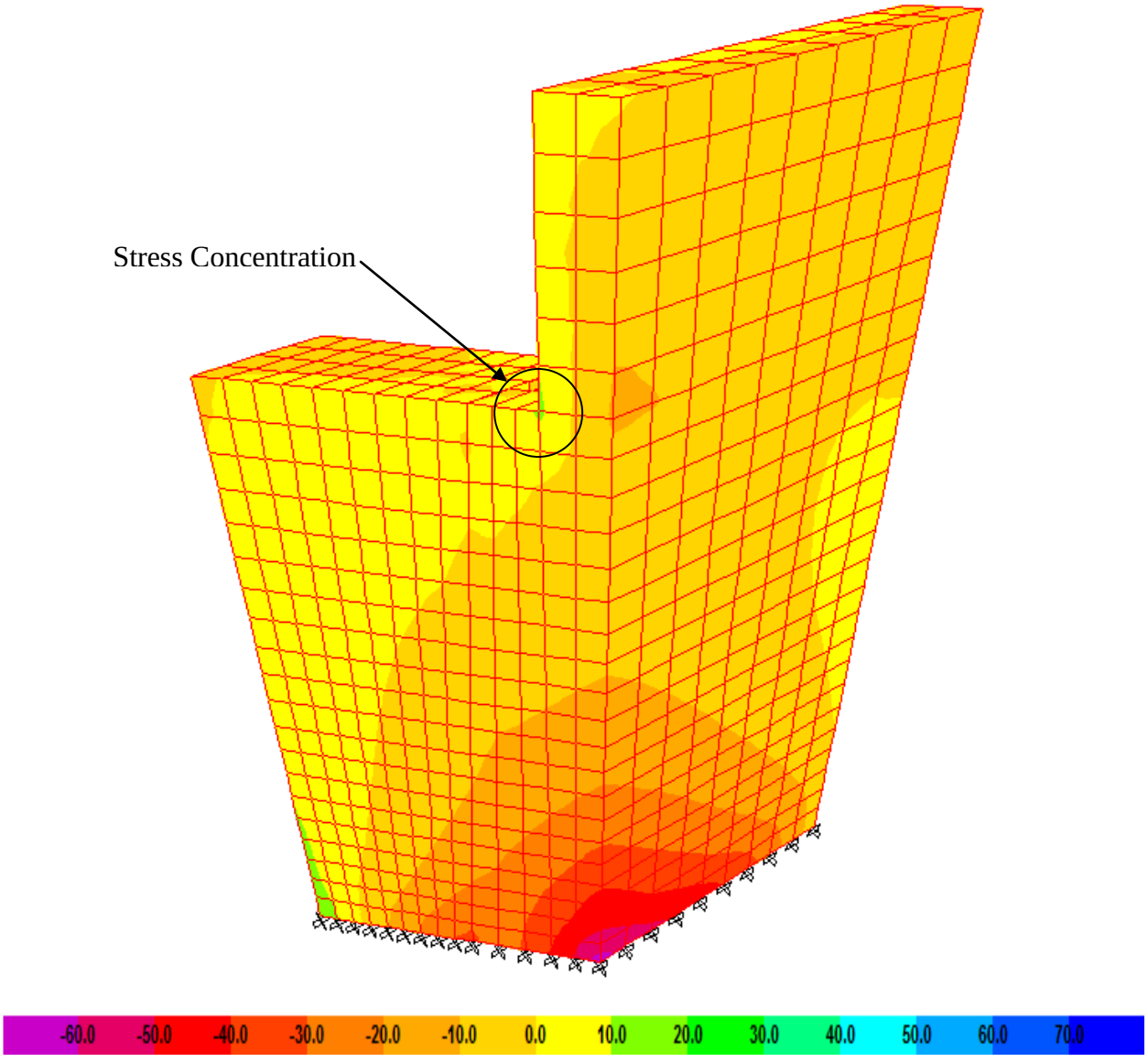

Figure 49: Front Side Stresses (ksi)

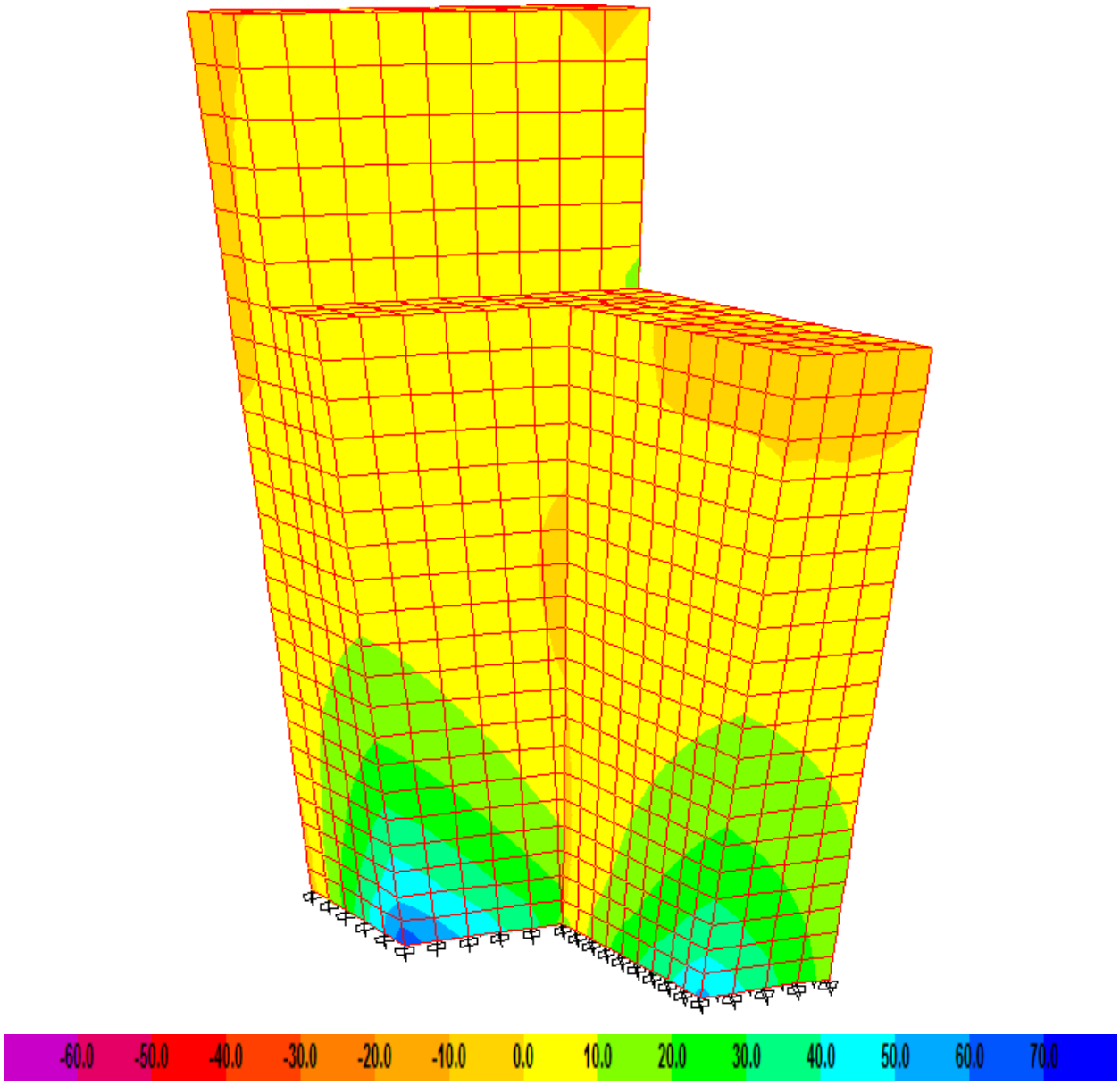

Figure 50: Backside Stresses (ksi)

Figure 51 shows the distribution of horizontal normal stresses on the front side of the wall panels.

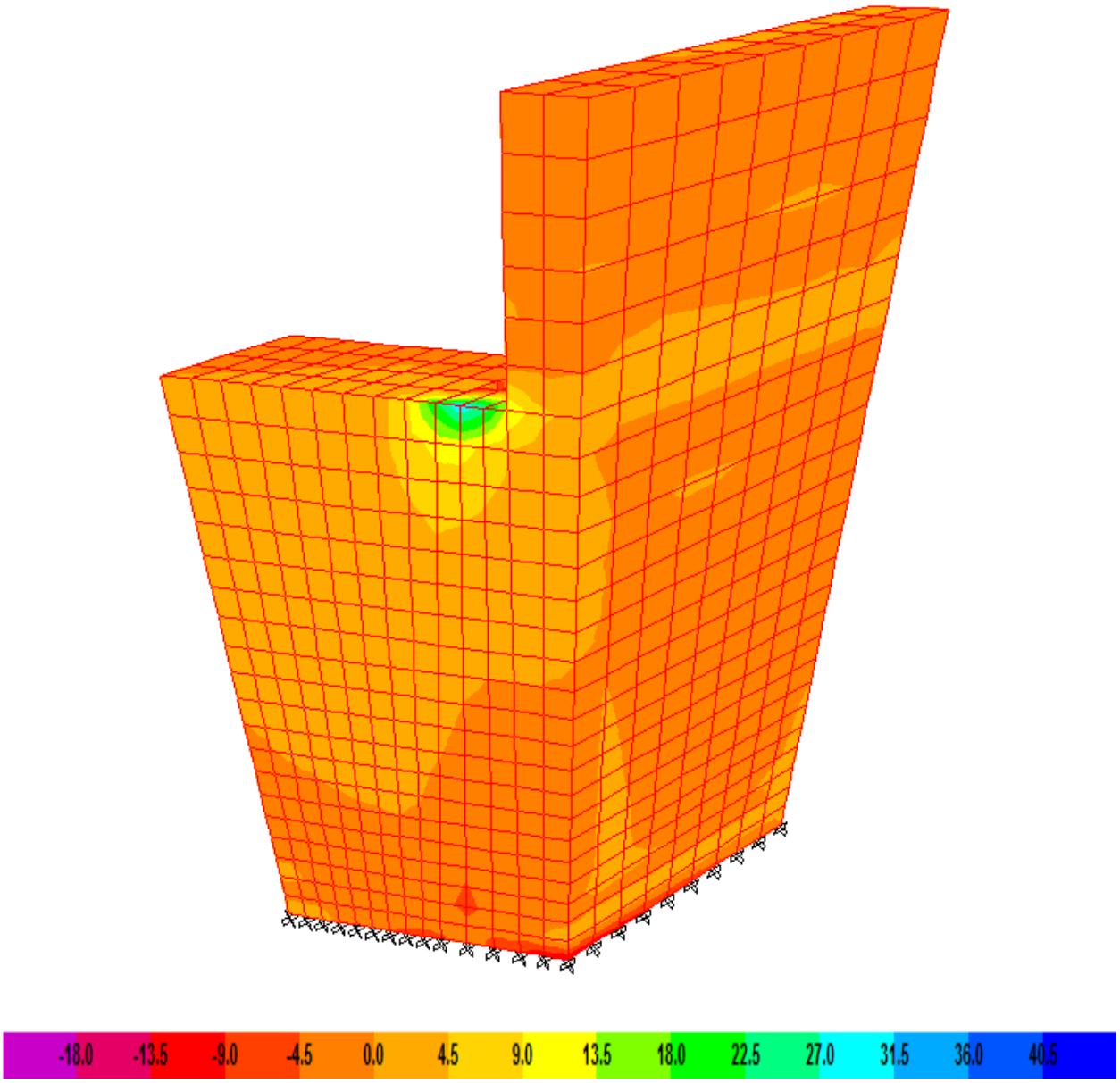

Figure 51: Front side Stresses (ksi)

CHAPTER 5: CONCLUSIONS

5.1 DEF -24 -0981

The data from the sensors showed that the average stress in the wingwall increased as the temperature increased. The magnitude of the stress however was not consistently associated with a specific temperature. This implies that other factors influence the temperature and stress relationship. Initially the stress distribution over the height of the wall appeared to be close to uniform for the lower portion of the wall and to be lower near the top of the wall. However, over time the stress distribution changed shape with a larger stress existing approximately 5.5' above the base of the wall. The stresses near the bridge were in general lower than the stresses further toward the approach slab. This would tend to support the theory of the diaphragm movement being related to the rotation of the bridge causing higher compression toward the soil side of the diaphragm.

The data from measuring the joint opening between the wingwall and diaphragm showed larger openings at lower temperatures. The largest total change in the joint was over 2 inches. In general, when the joint gap between the wingwall and diaphragm decreases the magnitude of the stress increased. However, the actual gap measurement did not directly correlate with a specific magnitude of stress. The behavior of the gap compared to the stress is likely due to the complex behavior exhibited at the wingwall/diaphragm interface caused by the thermal changes. The movement of the bridge's diaphragm at the interface is a combination of longitudinal sliding, movement in the direction of the skew into the wingwall, and rotation. All of these movements are also affected by the temperatures that vary in magnitude, duration, history, and location on the bridge. Therefore, the complex movement cannot be fully measured with the instrumentation installed only on the front face the wingwall/diaphragm interface.

The stress determined from the VW strain gages varied over the depth of the wingwall and in time. However, the majority of average stress measurements did not exceed 150 psi. This 150 psi stress is an extreme loading when considering the construction joint at the base of the wingwall (see Figure 52). Shear through the wingwall is not an issue, but bending at the base of the wingwall is a concern even with the #6 reinforcing bars on 12" centers. The tension caused

by bending is also on the surface of the wingwall that is not viewable for inspection. It is also difficult to determine how the stress from the diaphragm distributes along the length of the wingwall to lessen the effect of the bending. Soil on the outside of the wingwall can also assist in resisting the moment from the diaphragm.

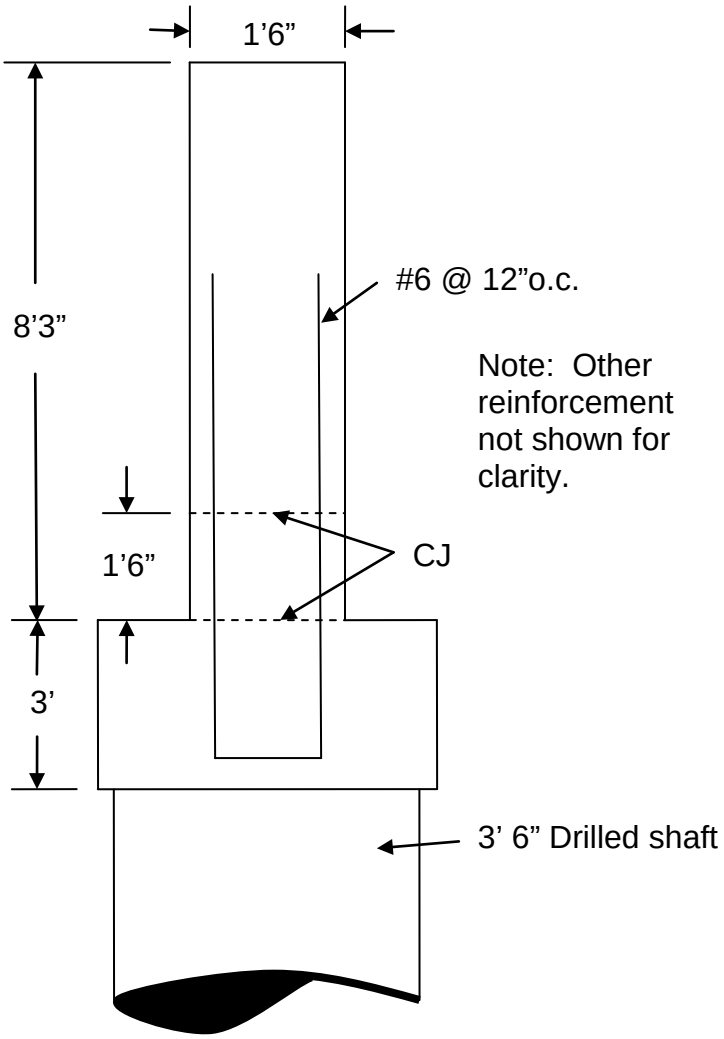

Figure 52: Wingwall Detail (DEF-24-0981)

5.2 MUS - 16- 0261

The data from the joint gap readings showed that the joint gap reduced under

higher temperatures and increased upon lower temperatures. The largest total movement of the joint over the sampling period occurred on the east bound bridge and was over 0.3". Slight changes in the tilt of the abutment walls and the wingwalls were found but they were very minimal.

The MUS-16-0261 bridge was constructed long before instrumentation was installed. Therefore, behavior from the instrumentation can only be discussed from the time of instrumentation. However, review of the plan details for the bridge provided some additional information (see Figure 53). The bearing retainer shown in the plan details to have a 0.25" clearance between the retainer and the plate at the bottom of the girder. The targets used to measure the eastbound bridge were installed in October and the largest movement of the joint was an opening of the joint of slightly less than 0.23". Closing of the joint was less than 0.13" the following July. If the capacity of the retainer was exceeded, it would have likely been the result of a bearing failure of the concrete at the bolt and concrete interface. Figure 54 provides an external view of the location of the bearing retainer and according to the District Bridge Engineer, the location has been patched. The spalling of the concrete could have been due to bearing failure of the concrete, especially considering the small amount of cover from the skew effect. Corrosion of the anchor bolts is likely occurring by evidence of the staining below the retainer location on the abutment wall.

Another issue is related to the bending of the wingwall caused by the force from the diaphragm. The reinforcement to resist the tensile force generated by the bending

consists of #5's at 18"o.c. In addition to the limited reinforcement, the minimum embedment shown is not sufficient for developing the full capacity of the reinforcement.

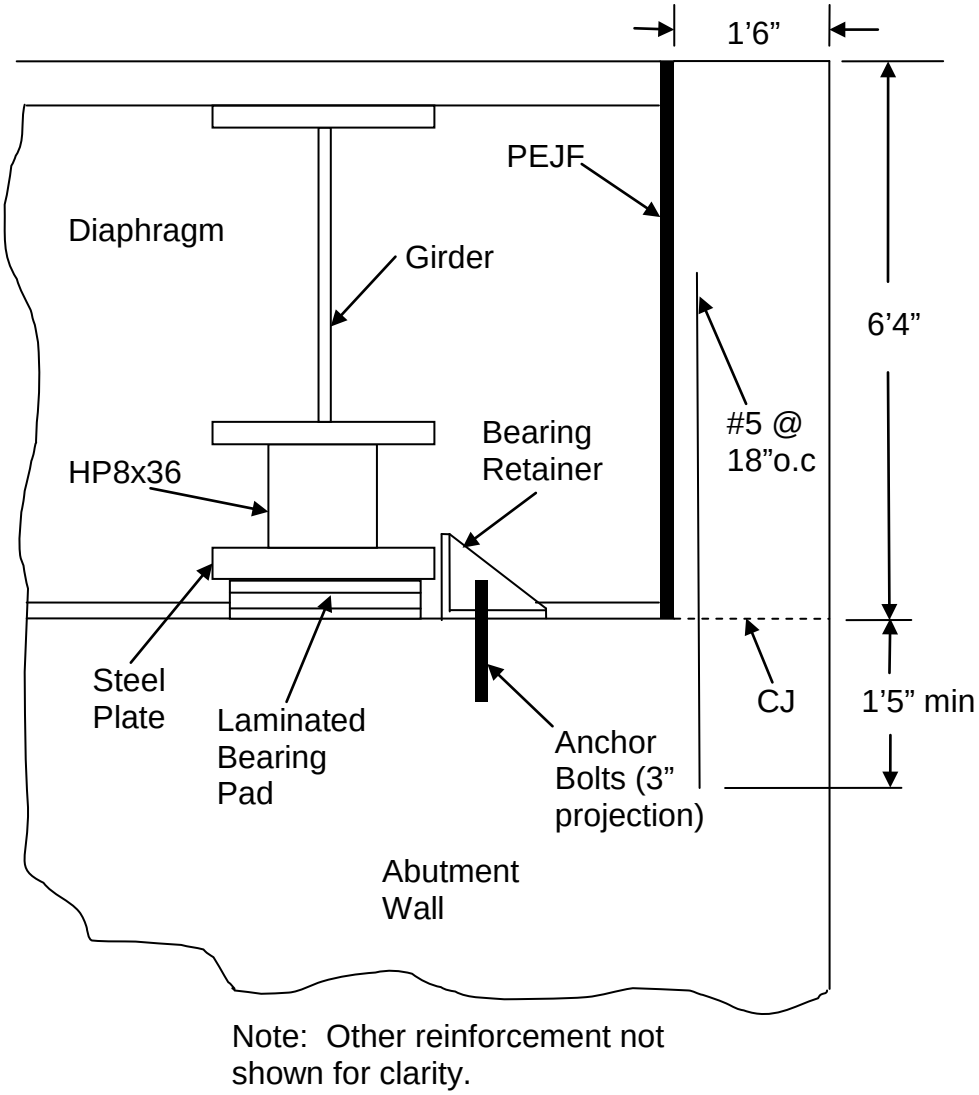

Figure 53: Wingwall Detail (MUS-16-0261)

Figure 54: Bearing Retainer (MUS-16-0261)

The results of the field data collected from both bridges and the analytical study show the behavior of the diaphragm to be very complex due to the numerous factors influencing the system.

CHAPTER 6: RECOMMENDATIONS

Based on the results of the following recommendations are made:

- Wingwalls in skewed semi-integral bridges which are turned back to run longitudinally with the bridge should account for the bending induced in the wingwall from stress in the wingwall/diaphragm interface generated by thermal expansion of the bridge.
- For the design of the wingwalls turned to run nearly parallel with the longitudinal axis of skewed semi-integral bridges should include a 100 psi loading at the wingwall/diaphragm interface from the thermal expansion of the bridge.
- Though analytical evaluations show that longer spans and higher skews than allowed by ODOT's BDM could be used, additional considerations for larger movements and stresses generated at the wingwall/diaphragm interface would need to be considered in designs.
- Vertical reinforcement in the wingwall near the bottom of the diaphragm should have sufficient embedment above and below to meet development length criteria of the reinforcement.
- Bearing retainers in diaphragms, if used, should assure adequate cover to avoid spalling of concrete. This is especially true of bridges with very high skews.
- Internal temperatures in the wingwall of the bridge can vary from ambient temperatures, making it difficult to estimate the affects of the thermal expansion of the bridge.
- The behavior of the wingwall/diaphragm interface is complex due to the combination of longitudinal sliding, movement in the direction of the skew into the wingwall, and rotation. All of these movements are also affected by the temperatures that vary in magnitude, duration, history, and location on the bridge.
- The construction process, such as the placement of the deck and diaphragm, likely affects the wingwall/diaphragm interface behavior. Placement during high temperatures would initially reduce thermal expansion stresses.

CHAPTER 7: REFERENCES

Bettinger, C.L. (2001), "Effects of Thermal Expansion on a Skewed Semi-integral Bridge," A thesis submitted in partial fulfillment of the requirements for the degree of Master of Science, Department of Civil Engineering, Ohio University, Athens, Ohio.

Bowles, J.E. (1996), Foundation Analysis and Design, 5th Ed., McGraw-Hill, New York.

Bridge Design Manual. (2000). Ohio Department of Transportation, Office of Structural Engineering, Columbus, Ohio.

Bridge Design Manual. (2007). Ohio Department of Transportation, Office of Structural Engineering, Columbus, Ohio.

Budhu, M. (2008), Foundations and Earth Retaining Structures, John Wiley and Sons, Ltd, Chichester, West Sussex, United Kingdom.

Burke, M.P., Jr., (2009), Integral and Semi-Integral Bridges, Wiley-Blackwell, John Wiley & Sons, Ltd, Chichester, West Sussex, United Kingdom.

Burke, M.P., Jr., and Gloyd, S. (1996). "Semi-integral bridges: A revelation," Paper presented at The Transportation Research Board's 75th annual meeting, Washington, D.C., January.

Burke, M.P., Jr., (1994A), "Semi-integral Bridges: Movements and Forces," *Transportation Research Record 1460*, Transportation Research Board, Washington, D.C., 1-7.

Burke, M.P. (1994B), "The Longitudinal, Lateral and Rotational Movement of Semi-integral Bridges," Paper presented at The Transportation Research Board's 73rd annual meeting, Washington, D.C., January.

MacGregor, J.G., and Wight, J.K., (2005), Reinforced Concrete Mechanics and Design, 4th edition, Pearson Prentice Hall, Upper Saddle River, NJ.

Masada, T. (2007). *Monitoring of bridge abutment walls at state route 33 over East State Street. Athens, OH.* Department of Civil Engineering, Ohio University, Athens, Ohio.

Metal Suppliers Online (2008). "Material property data."
< http://www.suppliersonline.com> (Feb. 11th, 2008)

Metzger, A.T. (1995). *Measurement of the abutment forces of a skewed semi-integral bridge as a result of ambient temperature change.* Master's Thesis, Department of Civil Engineering, Ohio University, Athens, Ohio.

Omega Engineering Inc. (2007). *Omega temperature measurement handbook,* 6th Ed., Omega Engineering Inc., Stamford.

Sargand, S. M., Masada, T., and Engle, R. (1999). "Spread footing foundation for highway bridge applications." *Journal of Geotechnical and Geoenvironmental Engineering,* 373-382.

Shehu, J., (2009), "Evaluation of the Foundation and Wingwalls of Skewed Semi-Integral Bridges with Wall Abutments," A thesis submitted in partial fulfillment of the requirements for the degree of Master of Science, Department of Civil Engineering, Ohio University, Athens, Ohio.

Steinberg, E.P., Sargand, S.M., and Bettinger, C.L. (2004), "Forces in Wingwalls of Skewed Semi-Integral Bridges," Journal of Bridge Engineering, ASCE, Nov/Dec, pp. 563-571.

Steinberg, E.P. and Sargand, S.M., (2001), "Forces Exerted in the Wingwalls of Skewed Semi-Integral Bridges," Final Report submitted to the U.S. Department of Transportation, Federal Highway Administration and the Ohio Dept. of Transportation, Ohio Research and Transportation Institute (ORITE), Department of Civil Engineering, Ohio University, Athens, Ohio.